AGU ADVANCING EARTH AND SPACE SCIENCES

Earth and Space Science

RESEARCH ARTICLE
10.1029/2023EA002872

Formation and Dynamics of a Coherent Coastal Freshwater Influenced System

Benjamin I. Barton[1], Michela De Dominicis[1], Rory O'Hara Murray[2], Judith Wolf[1], and Alejandro Gallego[2]

[1]National Oceanography Centre, Liverpool, UK, [2]Marine Directorate, Scottish Government, Aberdeen, UK

Key Points:

- Our simulation accurately resolves coastal freshwater due to its variable resolution
- A coastal salinity front is found west of Orkney with periodic release of its freshwater east of Orkney
- The movement of freshwater into and away from the coastal region is influenced by salinity driven currents and wind

Correspondence to:

B. I. Barton,
benbar@noc.ac.uk

Citation:

Barton, B. I., De Dominicis, M., O'Hara Murray, R., Wolf, J., & Gallego, A. (2024). Formation and dynamics of a coherent coastal freshwater influenced system. *Earth and Space Science*, *11*, e2023EA002872. https://doi.org/10.1029/2023EA002872

Received 15 MAR 2023
Accepted 8 DEC 2023

Author Contributions:

Conceptualization: Michela De Dominicis, Rory O'Hara Murray, Judith Wolf
Data curation: Benjamin I. Barton, Michela De Dominicis
Formal analysis: Benjamin I. Barton
Funding acquisition: Michela De Dominicis, Rory O'Hara Murray
Investigation: Benjamin I. Barton
Methodology: Benjamin I. Barton, Michela De Dominicis
Project Administration: Michela De Dominicis, Rory O'Hara Murray
Resources: Michela De Dominicis, Rory O'Hara Murray
Software: Benjamin I. Barton

Abstract On the Northwest European Shelf rivers provide freshwater to the coastal seas. This coastal freshwater can be misrepresented in ocean models without effective coastal resolution. This leaves an unanswered question; is freshwater retained around Scotland and what affects its variability? Here, we deploy and run an unstructured model with enhanced coastal resolution to simulate the Northwest European Shelf from 1993 to 2019, the Scottish Shelf Water-Reanalysis Service (SSW-RS) long-time run. The unstructured nature of the model grid means it more accurately captures a "bubble" of Coastal Water than a 7 km structured grid model (the Atlantic Margin Model 7 km). Surface salinity in the SSW-RS shows salinity fronts within 80 km of the coast around west and north Scotland that disintegrates east of Orkney. There are periods characterized by high coastal salinity when freshwater is more actively advected away from the coast. Empirical orthogonal function statistical analysis shows the first two modes in surface salinity account for 66% of the variance. The first mode correlates with North Atlantic Oscillation and the salinity driven velocity variability which change the salinity through advection and diffusion. The second mode correlates with Ekman transport variability where the north of Scotland acts as a wedge causing bipolar dynamics either side. Freshwater is trapped in the west, while saline water from the north reduces the freshwater pathway to the North Sea. This is important for salinity distribution, stratification in the North Sea, marine habitats and frontal transport.

Plain Language Summary The outflow of riverwater into the sea around Scotland is important for marine habitats, nutrient concentrations and the transport of pollution or planktonic larvae. The response of the sea to the sum of all river outflow is often missed in simulations of the ocean and leaves questions about how much water is retained near the coast and when it can escape. In our ocean simulation the Scottish Shelf Water-Reanalysis Service long run, we tackle this problem with high coastal resolution and an extensive river data set. Our simulation shows an improvement in salinity over a coarser resolution model of the same region around Scotland. Generally fresh, river-sourced water is retained by a front within 80 km of the coast around Scotland to the west of Orkney but this pattern is disrupted to the east of Orkney. Statistics show the majority of the variability in the freshwater around Scotland goes through stages at the time period of years when is it captured close to the coast and stages when it is more able to move away from the coast. This is found to correlate with density driven currents and the wind speed which uses the north of Scotland as a wedge for the water, causing bipolar dynamics either side.

1. Introduction

When freshwater from rivers enters the ocean, the surrounding coastal area is often referred to as a region of freshwater influence (ROFI) or river plume. These areas are important for productivity and exchange of water properties such as nutrients, pollutants, sediments and carbon between coast and offshore environments (Simpson, 1997). Rivers are a key source of freshwater and buoyancy in coastal regions and can set up a vertical and/or horizontal density gradient (Chapman & Lentz, 1994). The vertical density gradient is known as a surface-trapped plume, while the horizontal density gradient is known as a slope-controlled plume and depends on the bottom slope gradient (Fong & Geyer, 2002; Lentz & Helfrich, 2002; Munchow & Garvine, 1993). The horizontal density gradient forms a coherent front parallel to the coast with a density driven current/jet in geostrophic balance that can trap freshwater close to the coast. These fronts are important for understanding how far and how fast pollutants, nutrients or planktonic larvae might be transported away from the coast or how long they may be retained in the coastal area (Henry et al., 2018; Rabe et al., 2020). This is important for the salinity distribution, stratification in the North Sea and marine habitats (Lewis & Dadson, 2021).

Supervision: Michela De Dominicis, Judith Wolf
Validation: Benjamin I. Barton
Visualization: Benjamin I. Barton
Writing – original draft: Benjamin I. Barton
Writing – review & editing: Benjamin I. Barton, Michela De Dominicis, Rory O'Hara Murray, Alejandro Gallego

Unlike thermal buoyancy, riverine freshwater is present year round and provides a source of buoyancy to coastal seas. The thermal and haline fronts do not follow the same spatial pattern or temporal variability although they can interact in the summer (Hill & Simpson, 1989). When the riverine freshwater enters the sea it mixes with saline sea water in the energetic coastal and estuarine environment to produce a coastal sourced water that is sometimes referred to as Scottish coastal waters which we will call Coastal Water (CW) (Salinity <34.5 g/kg) and is less saline than offshore Atlantic Water (AW) (Salinity >35 g/kg) following the results and definitions of Jones et al. (2018, 2020); Inall et al. (2009). The sea water that is diluted with freshwater can be retained in coastal seas providing a store of lower salinity water. Salinity can be represented as Freshwater Content (F), which is the amount of freshwater required to dilute the sea water salinity (S) from a reference value (S_{ref}) often taken as a salinity of 35 g/kg using the equation $F = (S_{ref} - S)/S_{ref}$. This low salinity water can be removed from the near-shore environment by advection or diffusion, though it will only cause a noticeable concentration or dilution change in salinity where it can be replaced by sea water with a higher or lower concentration of salt.

The Northwest European Shelf and Scottish Waters have been intensely studied for aquaculture, coastal flooding events and tidal energy extraction (De Dominicis et al., 2017; De Dominicis, O'Hara Murray, et al., 2018; Rabe et al., 2020; Zijl et al., 2013). Parts of the Northwest European Shelf become seasonally stratified, with thermal tidal mixing fronts forming in summer, dependant on the bathymetry, current velocity and buoyancy forcing (Meyer et al., 2011). When seasonal stratification is eroded in winter, variability in North Sea transport has been shown to be largely wind driven (Holt & Proctor, 2008; Sündermann & Pohlmann, 2011). The winter wind driven residual transport is correlated with the North Atlantic Oscillation index in winter (r-value = 0.59), and has been shown to affect the interannual variability in water temperature (Inall et al., 2009; Mathis et al., 2015). The freshwater input from rivers is an active driver of year-round coastal current transport and should be included in models for accurate coastal dynamics (Sentchev & Korotenko, 2005; Sheehan et al., 2017). Individual rivers and associated ROFIs have been studied in the Northwest European Shelf but the variability in the sum of this coastal freshwater has not (de Brye et al., 2010; Palmer, 2010; Polton et al., 2011; Simpson, 1993; Souza & Simpson, 1997).

In this paper we would like to answer the question: is freshwater retained around Scotland and what affects its variability? To answer this question improvements have been made to the Scottish Shelf Model (SSM) which has been in iterative development since 2012 (De Dominicis et al., 2017; De Dominicis, O'Hara Murray, et al., 2018; Wolf et al., 2016). Its strength is the use of an unstructured grid focusing higher resolution cells on coastal areas based on Finite Volume Community Ocean Model (FVCOM) (Chen et al., 2003). Up to present, this has been a climatology run model forced with climatology atmospheric data, boundaries, rivers and tides. This has been used for addressing the interaction between Scottish lochs and the marine environment (Rabe et al., 2020) and estimating tidal energy at various sites (De Dominicis et al., 2017; De Dominicis, Wolf, & O'Hara Murray, 2018). In this study we present the latest version of the Scottish Shelf Water-Reanalysis Service (SSW-RS), which is a 27 year hindcast with the addition of forcing from a larger river data set, the Baltic Sea open boundary, ERA5 surface forcing and sea surface temperature (SST) assimilation. While the high resolution unstructured grid is expected to give more accurate results than a coarser model (Bricheno et al., 2014), we will test the improvement against a coarser model with temperature-salinity (T-S) profile assimilation (O'Dea et al., 2017). The methods are stated in Section 2, validation of the SSW-RS long-time run is shown in Section 3 along with analysis of coastal freshwater, there is a discussion in Section 4 and the conclusion is in Section 5.

2. Methods

2.1. The Scottish Shelf Water-Reanalysis Service

We now detail the model set up for SSW-RS the SSM Version 3.02 which has been run from 1 January 1993 to 31 December 2019 (27 years) (Barton et al., 2022) (see Data Availability Statement). The SSW-RS uses the FVCOM4.0 unstructured grid hydrodynamic model (Chen et al., 2003). The domain is based on the SSM grid described by De Dominicis et al. (2017), De Dominicis, O'Hara Murray, et al. (2018) with variable resolution from 0.5 km at the coast to 20 km at the Atlantic Ocean boundary (Figure 1a). The domain contains 267,744 nodes, 521,193 elements. The vertical levels in FVCOM use a σ-s hybrid coordinate system (terrain following), here implemented with 20 depth levels. The depth level are evenly distributed over the water column where the height of the free surface is <120 m. In water with height ≥120 m, the top five depth levels are fixed at 3, 9, 16, 23 and 30 m below the surface, while the bottom two depth levels are fixed at 6 and 12 m above the bottom. The

10.1029/2023EA002872

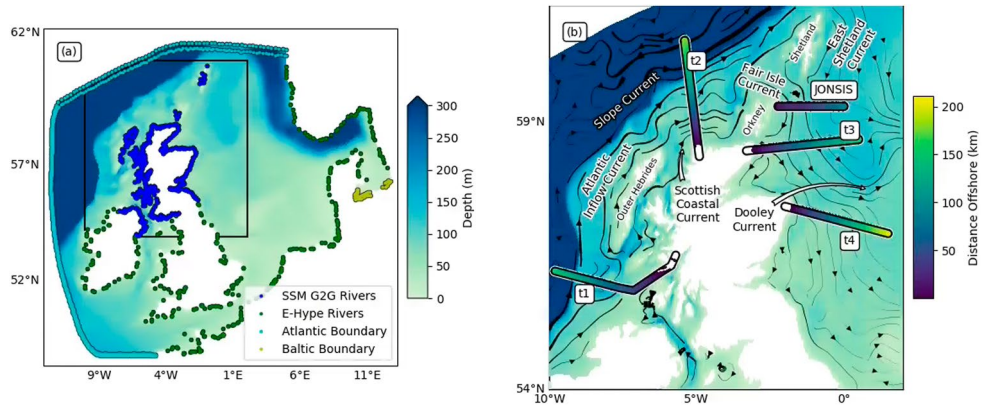

Figure 1. (a) Model boundary nodes are marked by light-blue points for Scottish Shelf Model (SSM) Atlantic boundary and the additional Baltic boundary nodes in Scottish Shelf Water-Reanalysis Service (SSW-RS) are marked by light-green points. The G2G river nodes used in SSM are shown in dark-blue and the additional E-Hype river nodes in SSW-RS are marked by dark-green points. Model bathymetry shown in color. The black lines show the empirical orthogonal function analysis region, zoom in (b). (b) Map with color shading showing distance away from the coast along the transects. Transects are labeled clockwise around Scotland from the west t1, t2, Joint North Sea Information System, t3 and t4. The areas outlined in black have widths of 15 km. The background color is the bathymetry as in (a). The streamlines show the residual currents with strength indicated by width.

bathymetry has been updated to European Marine Observation and Data Network which has been adjusted from lowest astronomical tide to mean sea level. In SSW-RS, the bathymetry data has been interpolated, smoothed at sharp gradients and had some alterations at estuaries to make the water column deeper depending on the volume flux of the respective river (Tonani et al., 2019). The minimum estuary node depths are 5, 10, 15, 25, and 30 m for rivers with maximum flux <50, <150, <300, <500, and >500 m^3/s, respectively.

The vertical turbulent mixing was parameterized by the General Ocean Turbulent Model coupled to FVCOM (Burchard, 2002). The horizontal mixing used the Smagorinsky parameterization with a constant horizontal diffusivity value of 0.2 m^2/s (Smagorinsky, 1963). Minimum bottom friction drag coefficient is a constant, set at 0.005 and length scale 0.01 m as this was shown to give the best tidal current and height validation on the North-west European Shelf for the updated bathymetry.

In addition to the open Atlantic boundary, SSW-RS has an open Baltic Sea boundary (Figure 1a). The boundary forcing used for both boundaries is the FVCOM "indirect" nesting scheme which contains elevation (including tidal elevation), velocity, temperature and salinity. This is applied over 2 layers of nodes and 1 layer of elements lining the boundary to give a weighted relaxation zone where SSW-RS variables are adjusted towards the boundary forcing.

The model's Atlantic Ocean facing open ocean boundary was forced by TPXO9-atlas harmonic tides for hourly current speed and sea surface height (SSH). The TPXO9-atlas tidal model provides global tidal harmonics at 1/30 degree resolution (Egbert & Erofeeva, 2002, 2020). The SSH and velocity harmonics used were M2, M4, MN4, MS4, S2, N2, 2N2, K1, K2, O1, P1, Q1 (see Data Availability Statement). These tidal harmonics were combined with daily forcing for temperature, salinity, residual (non-tidal) current speed and residual SSH from the Atlantic-European North West Shelf Ocean Physics Reanalysis. The latter is a regional reanalysis implementation of the Atlantic Margin Model 7 km (AMM7), a NEMO model implementation covering the Northwest European Shelf at 7 km resolution (O'Dea et al., 2017; AMM7-Team, 2022). Daily mean data is available between 1992 and 2019 for temperature, salinity, SSH, eastward velocity and northward velocity. The Atlantic-European North West Shelf Ocean Physics Reanalysis (which we will refer to as AMM7) assimilates SST and in situ T-S profiles and it uses the atmospheric forcing from the European Centre for Medium-Range Weather Forecasts (ECMWF) data set ERA5 (ECMWF Reanalysis fifth generation). A full description of the model can be found in (O'Dea et al., 2012; O'Dea et al., 2017) (see Data Availability Statement).

For the Baltic Sea facing open ocean boundary, the Baltic Sea Physics Reanalysis data was used for daily temperature, salinity, and residual current speed. SSH was forced by the hourly Baltic Sea Physics Reanalysis data which includes tide height. The Baltic Sea Physics Reanalysis is also a regional NEMO implementation

(Baltic-Sea-Physical-Reanalysis-Team, 2020; Hordoir et al., 2019). It has 4 km resolution covering the Baltic Sea and eastern North Sea. Daily mean temperature, salinity and velocity was used and hourly instantaneous SSH. The model assimilates SST and in situ T-S profiles. It had atmospheric forcing from ERA-Interim (see Data Availability Statement). The residual current speeds for the Baltic boundary were supplemented with tidal currents from TPXO9-atlas tidal harmonics. All daily boundary forcings were linearly interpolated to hourly data and spatially interpolated onto the nesting boundary nodes and elements points.

The model is mostly initialized with AMM7 accompanied by Baltic Sea Physics Reanalysis data for the respective areas. The model was give 1 month of spin up before January 1993 when output are available for use.

ERA5 is an atmospheric reanalysis data set from the ECMWF (Hersbach et al., 2018, 2020). ERA5 atmospheric data was used in SSW-RS for surface forcing of mean sea level pressure, precipitation, evaporation, surface air temperature, thermal radiation, solar radiations and wind velocity at hourly intervals. This is a global 30 km resolution data set with hourly atmospheric variables (see Data Availability Statement). These data fields were spatially interpolated onto the model grid. The sensible and latent heat fluxes have been calculated by the COARE2.6 (Coordinated Ocean Research Experiments) air-sea flux algorithm built into FVCOM (Fairall et al., 1996).

Daily satellite SST was assimilated from the Ocean Data Analysis System for Marine Environment and Security for the European Area (ODYSSEA). ODYSSEA is a gridded nighttime satellite SST data set from the Northwest European Shelf (Autret et al., 2019; ODYSSEA-Team, 2020). It is based only on satellite data and does not include in situ data. An empirical correction of 0.17 K converted satellite skin SST to foundation temperature. It has 0.04 degree resolution and is available as daily mean data (see Data Availability Statement). ODYSSEA data were spatially interpolated onto the model grid. The nudging data assimilation method was used that adjusts the temperature based on weighting that is dependent on the distance in time, space, depth and temperature between observation and model (Chen et al., 2003). The daily interval nighttime SST was assimilated between the times 10:30 p.m. and 1:30 a.m. This used the FVCOM gridded data assimilation routine to moderate the water temperature above the maximum vertical density gradient found between 2 and 100 m.

In the SSM climatology model the climatology river volume flux was provided by the Centre for Ecology and Hydrology (CEH) Grid-to-Grid (G2G) model (Bell et al., 2018) and only covered the coastline of Scotland and Northern Ireland (Figure 1a). This data set has a high spatial resolution, 577 rivers. The European-Hydrological Predictions for the Environment (E-HYPE) river data set is a model reanalysis that has daily river volume flux and temperature for the whole model domain from the Swedish Meteorological and Hydrological Institute (SMHI) (Arheimer et al., 2019; E-HYPE-Team, 2020). This is model reanalysis with 230 water gauging sites and 215 km^2 resolution. In the European data set there are 3032 E-HYPE river discharge points. The data set provides daily volume flux and temperature (see Data Availability Statement). E-HYPE has lower spatial resolution in Scotland and Northern Ireland than the G2G data. The two data sets were combined to maintain the spatial resolution but introduce daily variability and give river fluxes outside of Scotland and Northern Ireland. This was accomplished by matching rivers in the two data sets in the overlapping area in Scotland and Northern Ireland. First a climatology of E-HYPE fluxes was calculated. The nearest E-HYPE river to each G2G river was found. Then any additional E-HYPE rivers within 10 km of the closest E-HYPE river were identified. Of the identified E-HYPE rivers, a regression value is calculated with the E-HYPE flux climatology and G2G flux climatology. The E-HYPE river with the greatest regression value and closest order of magnitude to the mean river flux was selected. Given the more numerous G2G rivers, often multiple G2G rivers were matched to an E-HYPE river. An intercept-free linear regression model was calculated for the matched rivers and the temporally variable E-HYPE river flux was then scaled to the appropriate volume flux at the G2G discharge location. This means total flux of the E-HYPE data is maintained but distributed over a greater number of discharge locations. E-HYPE river temperature was also transferred to the respective G2G locations. The combined data set of Scottish-Northern Irish rivers with Northwest European Shelf rivers contains daily volume flux and temperature for 912 rivers in the model domain, 577 of these are in Scotland and Northern Ireland. With the compiled river data set, the rivers were attached to the nearest model node. Rivers attached to the same model node have had their volume flux summed and a weighted average of temperature calculated. Rivers with maximum volume flux greater than a threshold of 1000 m^3/s were divided over a number of nodes.

2.2. Validation and Analysis

For validation of model temperature and salinity, comparisons are made to the Coriolis Ocean database for ReAnalysis (CORA) in situ T-S profile data (see Data Availability Statement). The CORA T-S profile data set combines several sources of profiles into one quality controlled data set (Cabanes et al., 2013; Tanguy et al., 2020, 2022). Roughly 150,000 temperature profiles and 50,000 salinity are in the model domain between 1993 and 2019. Each profile was paired with the closest model node and at the closest time in the hourly model output. The model data was linearly interpolated into the depth levels of the observation data. The same paring was done with the AMM7 data which has lower coastal horizontal resolution than SSW-RS and climatology rivers but uses T-S profile assimilation. This was used for comparison with SSW-RS. A higher resolution NEMO model of the Northwest European Shelf exists, the Atlantic Margin Model 1.5 km (AMM15) (Guihou et al., 2018; AMM15-Team, 2022). An AMM15 analysis run with SST data assimilation overlaps our SSW-RS run only for 2019 (see Data Availability Statement). This was not long enough for a full comparison but we make use of the overlapping time by comparing with the available profiles. While the temperature profiles in 2019 were well spread around Scotland, unfortunately there were no salinity profiles around Scotland, only in the southern North Sea. The AMM15 data set used was forced by the operational ECMWF Numerical Weather Prediction model, climatological rivers, the lateral boundaries are from the Baltic Sea Physics Reanalysis (previously mentioned) and the 1/12° North Atlantic NEMO model (NATL12).

Further temporal comparisons are made to surface salinity data collected at Joint North Sea Information System (JONSIS) Line (JONSIS-Project, 2021; Larsen et al., 2016), a transect, that lies off the coast of Orkney 2.23°W to 0°W along 59.28°N, regular monitored by the Scottish Government's Marine Directorate. This line has been surveyed 1 to 5 times a year from 1960 to present for temperature and salinity (see Data Availability Statement).

Horizontal gradients in temperature and salinity can be used to identify the fronts that isolate areas with similar properties. On the unstructured SSW-RS grid the planar gradient was calculated from the linearly interpolated triangular grid (https://matplotlib.org/stable/api/tri_api.html). While this is different from the Green-Gauss theorem used by FVCOM, planar gradient achieves a very similar result and was more efficient for post-processing analysis. We make a comparison of the gradients with AMM7 used to force the model boundaries. For the plots of salinity gradient identifying front, the magnitude of the gradient in east and north directions was used for SSW-RS and AMM7.

To determine whether the fronts were slope-controlled or surface-trapped plumes, we estimate the ratio W_w/W_α which is the main criteria for a surface-trapped plume in the simplest form (Lentz & Helfrich, 2002). The ratio represents whether the bottom expression of the front is closer to the coast W_α or the surface expression of the front W_w. To do this, we calculated the surface to bottom density difference averaged over 1993 to 2019, and compare it against the surface expression of the salinity front. We confirm out estimate by calculating the residual bottom velocity perpendicular to the coast over 1993 to 2019 (Chapman & Lentz, 1994).

We take transects through the front to show their temporal variability. Four transects are used extending away from the Scottish coast oriented to gain maximum distance from the coast (Figure 1b). The transects were chosen to avoid islands, where possible, that may change the mixing and front location. The data were also binned by distance from the coast, where the width of the bin perpendicular to the transect is 15 km. This means our transects are as representative as possible of the average conditions around them.

To further investigate the frontal forcing at daily resolution, 1999 was selected as an example year because it has relatively average salinity front conditions and is between high and low North Atlantic Oscillation index. Over the year 1999, we used an FVCOM subroutine to calculate the 2D momentum balance components during model run-time (Chen et al., 2003). This was done at discrete points along our transects. We used the components of the momentum balance with the greatest contribution here. These were Coriolis force, barotropic pressure gradient force (PGF), baroclinic PGF, stress (combined surface and bottom), and advection of momentum. To break the combined stress into wind and bottom stresses, we calculate wind stress acceleration as $w = \tau/(\rho_0 H)$ where τ is wind stress, ρ_0 is the reference density taken as 1,025 kg/m^3 and H is the water depth. The wind stress has been converted from the nodes to the elements by calculating an element-centre value based on the average value for the nodes from which it is formed. We present the magnitude of the two momentum components u and v for each of the forces. Together these components define the acceleration/deceleration of water velocity and how the velocity is influenced by aspects of the physical environment.

To analyses the temporal and spatial variability in surface salinity around Scotland, empirical orthogonal functions (EOFs) were calculated with the singular value decomposition method (Thomson & Emery, 2014). The EOF analysis provides a wide view perspective on the collective system, as opposed to using transect sections alone which would only give discrete points. It enables us to understand the variability rather than just the balance of forces at the front. EOF analysis finds a spatial pattern and a temporal index referred to as the principal component (PC) from a field of data. The field can be divided into mathematically orthogonal modes each of which is independent. Each mode may be seen as oceanographic structures like circulation in the North Sea (Mathis et al., 2015) or atmospheric structures like the North Atlantic Oscillation (Hurrell & Van Loon, 1997). To find these modes, the eigenvalues and eigenvectors of an anomaly fields covariance matrix are computed. The eigenvectors represent the spatial patterns. The eigenvalues indicate the percentage of variance explained by each mode and the sum of all eigenvalues represents the total variance in the data. Oceanographic processes tend to exhibit low-frequency behavior, where the variance is concentrated in the first few modes. The PCs, are obtained by projecting the derived eigenvectors onto the spatial anomalies. This gives a timeseries of the amplitude of a mode. The limitations are the spatial patterns derived may depend on the region selected and modes must be orthogonal.

Our EOF analysis region is a box from 54°N to 61°N and 10°W to 2°E. Several steps were taken to normalize the salinity data at each grid cell before EOF analysis, (a) monthly means of salinity were calculated; (b) the seasonal cycle in salinity was averaged out with a 12-month running mean; (c) the mean salinity was removed; (d) the salinity was detrended; (e) salinity was divided by its respective standard deviation. These are the same methods used in Barton et al. (2018). Regressions were calculated between the PCs, current velocity (as u and v components) and river volume flux. These parameters were also averaged with a 12-month running mean. Significance of these regressions at 95% level were estimated with a two-tailed Welch's t-test. Given the regressions are made with 12-month running mean data, the effective degrees of freedom were used for significance estimation. The effective degrees of freedom were estimated from the auto-decorrelation timescale, $r \leq r_{\max}(1/e)$ where regression is r, e is Euler's number, peak regression is $r_{\max}$.

The PCs were regressed with a breakdown of the energy sources that force depth averaged currents. The regression values are calculated point-wise so the timeseries at each grid location is regressed with the respective primary component. For regression with velocities, each u and v component are regressed and combined to provide directional regression. The temporal regression values are then assembled into maps. The energy sources are the wind driven Ekman transport, the temperature and salinity drivers of density currents and the mass of water driven eustatic currents which we will refer to as *Ekman*, *T-Driven*, *S-Driven*, and *Eustatic* respectively. These energy sources are calculated as follows.

The baroclinic currents resulting from temperature and salinity variations can be classified in terms of α and β the coefficients for thermal expansion and haline contraction, respectively (Carmack, 2007; McDougall, 1987). The density contribution from temperature and salinity can be calculated as $\rho = \rho_0(-\alpha T + \beta S)$ where ρ_0 is the reference density taken as 1,025 kg/m^3, ρ is variable density, T is the conservative temperature and S is absolute salinity (Roquet et al., 2015). This equation is substituted into the density based thermal wind equation to separate the temperature and salinity based current forcing (Roquet et al., 2015).

The SSH used for the barotropic current comes from the steric height (integrated density) and eustatic height (integrated mass which can be derived form bottom pressure) (Armitage et al., 2016; Barton et al., 2020). Steric height (η_{st}) can be calculated as follows where g is gravitational acceleration, p_1 and p_2 are the ocean surface and bottom pressures in Pa, $\rho_{ref}(z)$ is a reference density calculated for $T = 0$°C and $S = 35$ with variable pressure:

$$\eta_{st} = \frac{1}{g}\int_{p_2}^{p_1} \frac{1}{\rho(z)} - \frac{1}{\rho_{ref}(z)} dp \tag{1}$$

This can be represented as temperature based thermosteric height (η_T) and salinity based halosteric heights (η_S) as $\eta_{st} = \eta_T + \eta_S$. Thermosteric height and halosteric height can be calculated in Equations 2 and 3 respectively where ϑ is the specific volume, and z_1 and z_2 are the ocean surface and bottom depth (Levitus et al., 2005).

$$\eta_T = \int_{z_2}^{z_1} \frac{1}{\vartheta}\frac{\partial \vartheta(z)}{\partial T}\Delta T\, dz \tag{2}$$

$$\eta_S = \int_{z_2}^{z_1} \frac{1}{\vartheta} \frac{\partial \vartheta(z)}{\partial S} \Delta S dz \tag{3}$$

The steric height based barotropic current can be subtracted from the barotropic current to leave the mass based *Eustatic* current. The thermosteric and halosteric height based currents are then added to the thermal wind current for temperature and salinity respectively. This means we accumulate density based current forcing together and calculate the *T-Driven* and *S-Driven* components.

The energy sources (*Ekman*, *T-Driven*, *S-Driven* and *Eustatic*) to the depth averaged currents can be represented by the following Equations 4 and 5:

$$\bar{u} = \underbrace{\frac{1}{f\rho_0}\frac{\partial \tau_y}{\partial z}}_{Ekman} + \underbrace{\left(\overline{\frac{1}{f\rho_0}\int_{z_2}^{z_1} \alpha \frac{\partial T(z)}{\partial y} dz} + \frac{g}{f}\frac{\partial \eta_T}{\partial y}\right)}_{T-Driven} - \underbrace{\left(\overline{\frac{1}{f\rho_0}\int_{z_2}^{z_1} \beta \frac{\partial S(z)}{\partial y} dz} - \frac{g}{f}\frac{\partial \eta_S}{\partial y}\right)}_{S-Driven} - \underbrace{\frac{g}{f}\frac{\partial(\eta + \eta_{st})}{\partial y}}_{Eustatic} \tag{4}$$

$$\bar{v} = -\underbrace{\frac{1}{f\rho_0}\frac{\partial \tau_x}{\partial z}}_{Ekman} - \underbrace{\left(\overline{\frac{1}{f\rho_0}\int_{z_2}^{z_1} \alpha \frac{\partial T(z)}{\partial x} dz} - \frac{g}{f}\frac{\partial \eta_T}{\partial x}\right)}_{T-Driven} + \underbrace{\left(\overline{\frac{1}{f\rho_0}\int_{z_2}^{z_1} \beta \frac{\partial S(z)}{\partial x} dz} + \frac{g}{f}\frac{\partial \eta_S}{\partial x}\right)}_{S-Driven} + \underbrace{\frac{g}{f}\frac{\partial(\eta - \eta_{st})}{\partial x}}_{Eustatic} \tag{5}$$

Where $\bar{u}$ is the depth averaged velocity, f is the Coriolis parameter, τ is wind stress in the x and y direction respectively and η is the surface elevation. The wind stress is divided by the full depth z because this is how it is calculated in FVCOM. This was calculated with functions from the Gibbs Sea Water function package (http://www.teos-10.org/pubs/gsw/html) (IOC et al., 2010). The equations presented above were used as an approximation of the variability in each energy source for regression purposes.

The freshwater budget was calculated to quantify the sources of freshwater to the region used in the EOF analysis. Equation 6 is the freshwater budget (Serreze et al., 2006).

$$F_{tr} = F_{vol} - (F_{surf} + F_{riv}) \tag{6}$$

The surface freshwater flux was calculated as $F_{surf} = P + E$, where E is evaporation, P is precipitation. F_{riv} is river runoff. F_{vol} is the freshwater volume change over time, calculated as $F_{vol} = d\left(\int\int\int((S_{ref} - S)/S_{ref})dx\,dy\,dz\right)/dt$, where S is salinity and S_{ref} is a reference salinity taken as 35 g/kg. We calculate the freshwater transport F_{tr} as the sum of F_{surf}, F_{riv} subtracted from F_{vol}, and would also be relative to S_{ref}. Positive values for the integrated fluxes represent flux into the ocean box.

A large portion of the model setup and analysis was completed with the use of functions in the Python FVCOM library PyFVCOM (Cazenave & Bedington, 2019) (see Data Availability Statement). The code used for post-processing the data is available online (Barton, 2023).

3. Results

3.1. Temperature and Salinity Validation

Spatial patterns, such as fronts, are captured by SSW-RS and can be compared with observations in climatology maps (Figure 2). The differences between the observations and SSW-RS are very subtle. The main difference here is 1°C cooler surface temperature in the model west of Scotland and to a lesser extent all across the region

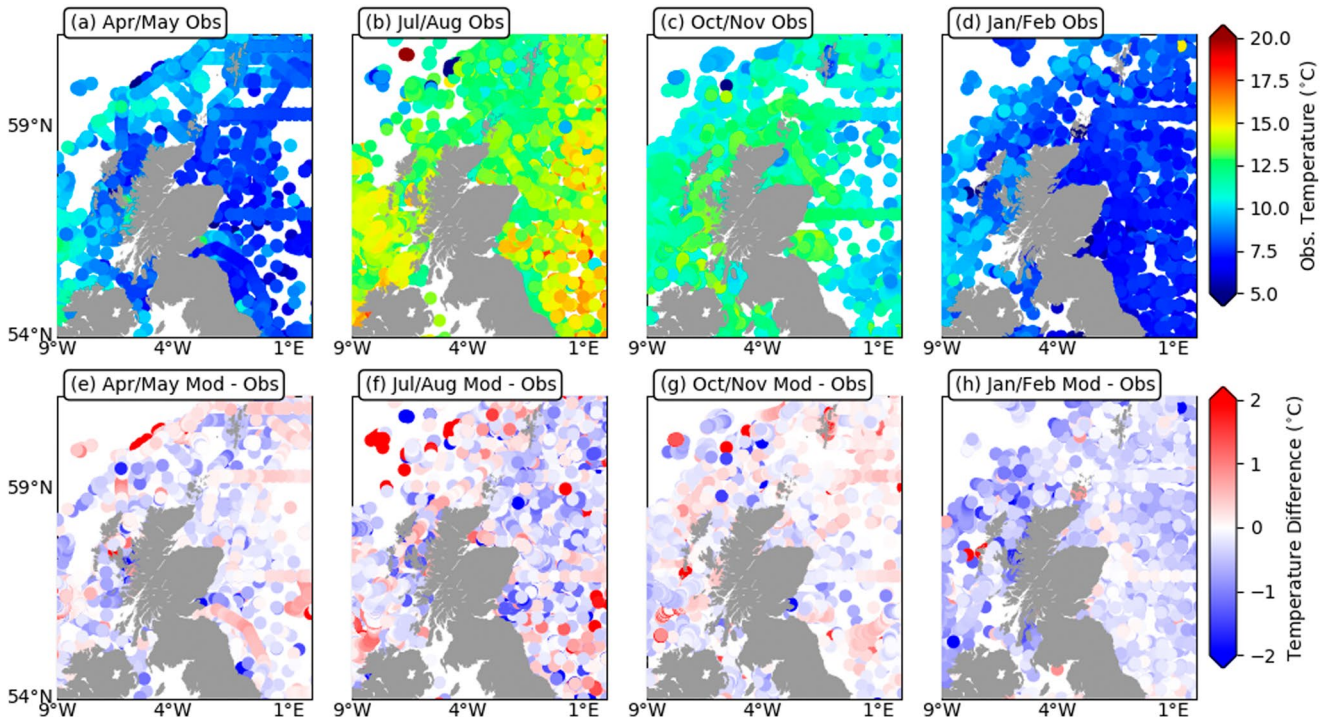

Figure 2. Water temperature for profiles averaged vertically over the upper 20 m. These profiles were collected between 1993 and 2019. (a–d) Show observations, (e, f) show model (Scottish Shelf Water-Reanalysis Service) values minus observations. The data are shown for 2 months in each case to avoid overcrowding but repeat sample locations will cover an earlier profile.

in January and February. A −0.5°C bias persists from April to August on the shelf. Given that SSW-RS has SST assimilation, it suggests the bias is coming from below the surface in the amount of heat advected into the region. Heat advection which is too small could be the result of the SST assimilation acting over too large a portion of the water column, resulting in too much heat loss. The temperature below 40 m shows similar agreement between SSW-RS and observations (not shown).

Spatial patterns in the climatology of salinity are captured in SSW-RS (Figure 3). The spatial patterns in salinity show good agreement between SSW-RS and observations with the fresher water in coastal regions forming a "bubble" of CW around Scotland with salinity <34.5 g/kg. In general the North Sea is 0.1 g/kg less saline in SSW-RS than observations and the Irish Sea is 0.3 g/kg more saline in SSW-RS than observations. There does not appear to be strong seasonality in salinity for the observations but there is some mild seasonality in SSW-RS most evident as 0.1 g/kg more saline conditions along the east coast of the UK in July/August. The weak seasonality is in agreement with Inall et al. (2009).

The T-S plots in Figure 4 show the concurrent properties. In both observations and SSW-RS the seasonal temperature and salinity changes in the water masses are in agreement. This shows the watermasses CW (S < 34.5 g/kg) and AW (S > 35 g/kg) following Jones et al. (2018). The lower salinity CW in SSW-RS accurately represents the matching fresher observation points. The CW then mixes with more saline AW in winter (see high density areas oriented horizontally in Figures 4a–4c). In winter, the observations and SSW-RS show two peaks in the number of points, one around 10°C, 35 g/kg salinity and the other around 8°C, 35 g/kg salinity. This represents the difference in temperature of AW between west and east of Scotland. Each winter peak has high density areas oriented horizontally which are associated with mixing lines with fresher CW. The AW points appear warmer in summer in SSW-RS than the observations. AMM7 properties are plotted for comparison (Figures 4c and 4g). Summer temperature of AW in AMM7 is also warmer than the observations. The main difference is the points nearest the coast in AMM7 do not have as much low salinity CW. This occurs in both summer and winter in AMM7, meaning it does not capture then low salinity end points of the winter mixing lines in SSW-RS and the observations. AMM7 is also deficient in low salinity water exiting the Baltic Sea (not shown).

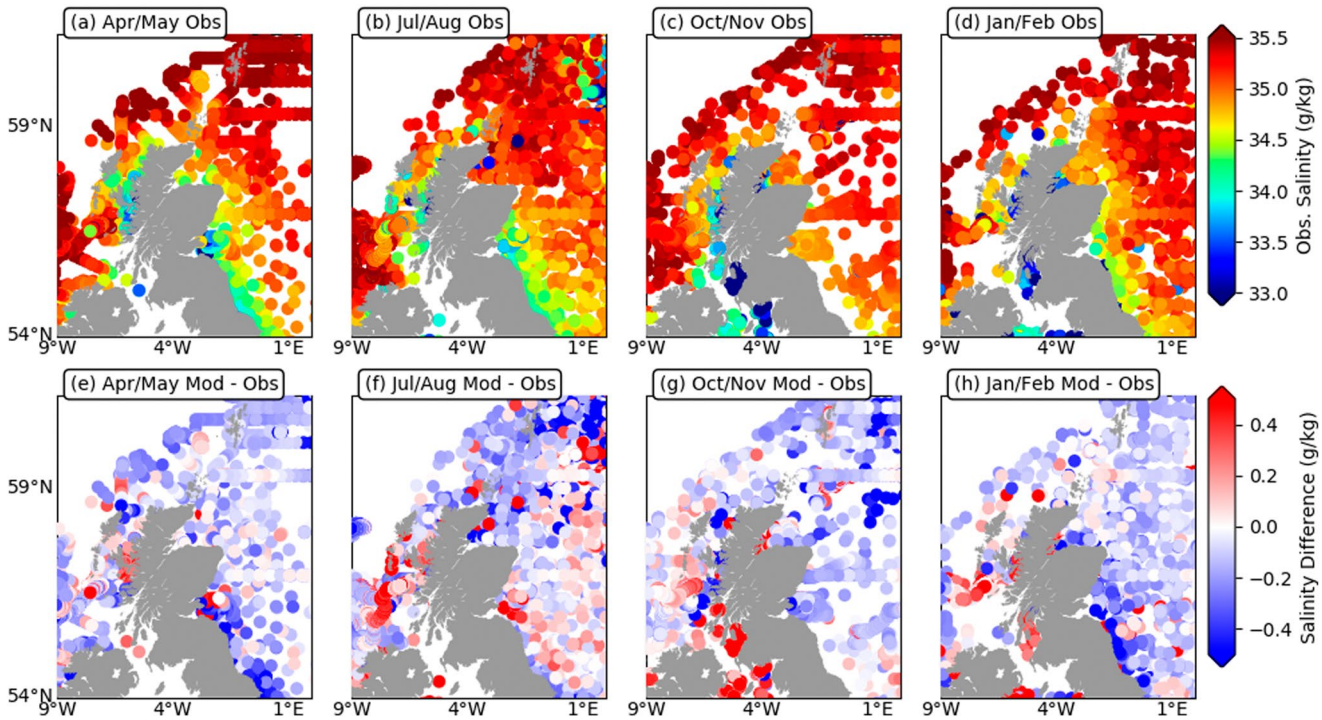

Figure 3. Salinity for profiles averaged vertically over the upper 20 m. These profiles were collected between 1993 and 2019. (a–d) Show observations, (e, f) show model (Scottish Shelf Water-Reanalysis Service) values minus observations. The data are shown for 2 months in each case to avoid overcrowding but repeat sample locations will cover an earlier profile.

Scatter plots show the difference between observed temperature and SSW-RS temperature, similarly for observed temperature and AMM7 (Figure A1). The temperature plots show a closer grouping between model and observation temperature at distances greater than 100 km from the coast. This is because the coastal environment, <100 km, is more dynamic with smaller mesoscale features that would be unlikely to coincide in the model (Figures A1a, A1b, A1e, and A1f in Appendix A). The salinity scatter plots highlight the low salinity values missing in AMM7 where SSW-RS has values on the 1-to-1 line from salinity 35 to 15 g/kg (Figures A1c, A1d, A1g, and A1h). SSW-RS has some offshore points (green points >100 km) with salinity <30 g/kg which should be more saline showing in some places the freshwater spreads too far offshore. In AMM7, these offshore points are clustered together closer to salinity of 35 g/kg. In AMM7, many of these salinity observations <25 g/kg are represented by salinity of >30 g/kg. The color scale shows the lowest salinity points in SSW-RS are within 25 km of the coast but there are some with <30 g/kg which are up to 125 km from the coast which represents advection of Baltic Water into the North Sea. The root mean square error between SSW-RS temperature and observation temperature is 0.026°C in winter and 0.013°C in summer. AMM7 temperature has a mean square error of 0.033°C in winter and 0.017°C in summer. For SSW-RS salinity against observations, the mean square error is 0.001 g/kg in winter and 0.001 g/kg in summer. AMM7 salinity against observations show a mean square error of 0.262 g/kg in winter and 0.181 g/kg in summer.

Using the 2019 data we make a comparison of the profile data set with the SSW-RS and the AMM15 data. Both data sets follow the spatial-temporal variability exhibited in the selection of profiles (note the applied offset Figure A2 in appendix). The temperature timeseries shows strong temperature variability in the water and then a gradual warming over the summer found in both SSW-RS and AMM7. The salinity profiles around the southern North Sea show locations with fresh CW and locations with more saline AW influence. The root mean square error for temperature in SSW-RS in winter 2019 is 0.0052 and 0.010°C in summer 2019. For AMM15 temperature, in winter 2019 error is 0.0068 and 0.012°C in summer 2019. SSW-RS salinity root mean square error in winter 2019 is 0.0003 g/kg and summer is 0.0004 g/kg. AMM15 salinity error in winter 2019 is 0.042 g/kg and summer is 0.059 g/kg. This shows SSW-RS is similar at simulating temperature to AMM15 but SSW-RS is much better at simulating salinity than AMM15 (although data is limited to the southern North Sea).

10.1029/2023EA002872

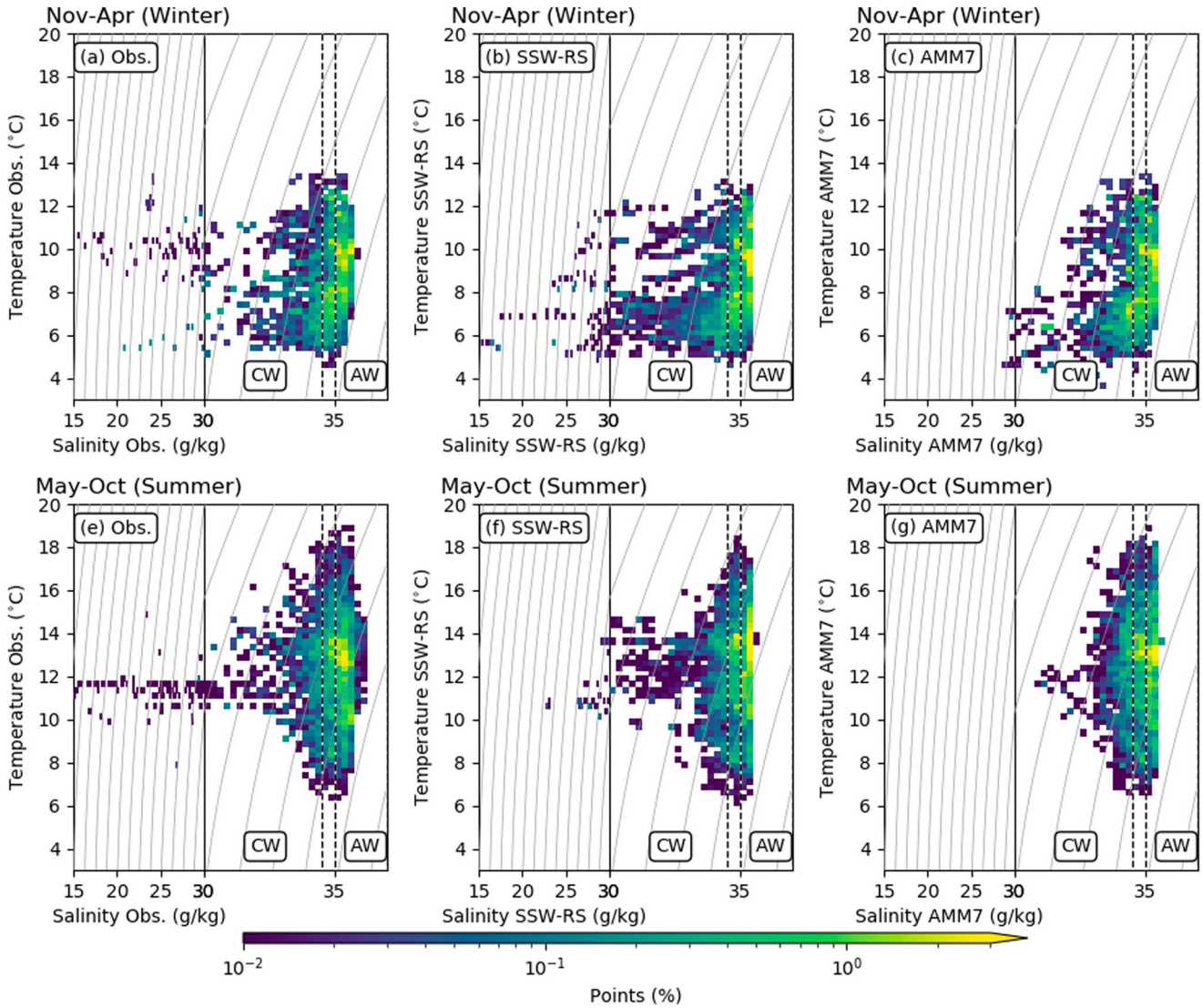

Figure 4. T/S diagrams for (a–c) November-April and (d–f) May-October, which we refer to as winter and summer respectively. (a), (d) Show observation values, (b) and (e) show Scottish Shelf Water-Reanalysis Service values, (c) and (f) show Atlantic Margin Model 7 km value. The water masses Coastal Water and Atlantic Water are shown with dashed lines at the boundary between them. Note, there is a non-linearity in the *x*-axis at salinity of 30 g/kg to highlight low salinity values. Color values shows the number of points per box as a percentage of the total. Data are shown for profiles on the shelf in depth <200 m and inside the analysis region 54°N to 61°N and 10°W to 2°E (Figure 1b).

3.2. Fronts

A 27 year mean of the SST and sea surface salinity reveals the long-term spatial patterns (Figures 5a and 5b). Generally, mean surface temperature is around 11°C south and west of Scotland, while averaging 10°C north and east of Scotland. Salinity reaches <32 g/kg (8.6% freshwater content relative to 35 g/kg) within 10 km of the coast and increases with distance offshore to >35 g/kg (0% freshwater content relative to 35 g/kg) at >100 km (for distances see Figure 1b). The low salinity water, at a distance <80 km from the coast, is a watermass documented by Balls (1985); Turrell et al. (1992), and Hill et al. (1997). There are persistent fronts in salinity at a distance <10 km from the coast (Figure 5d) that are also found in surface temperature (Figure 5c). These have potential to be slope-controlled plume fronts, we will return to this later. However, there are additional persistent salinity fronts found further offshore at a distance <80 km from the coast where salinity is around 34.6 g/kg and the horizontal gradient is 0.03 g/kg km, these are not present in the temperature fronts. These fronts could also be slope-controlled plume fronts and are strong enough to be a prominent horizontal density gradient (not shown).

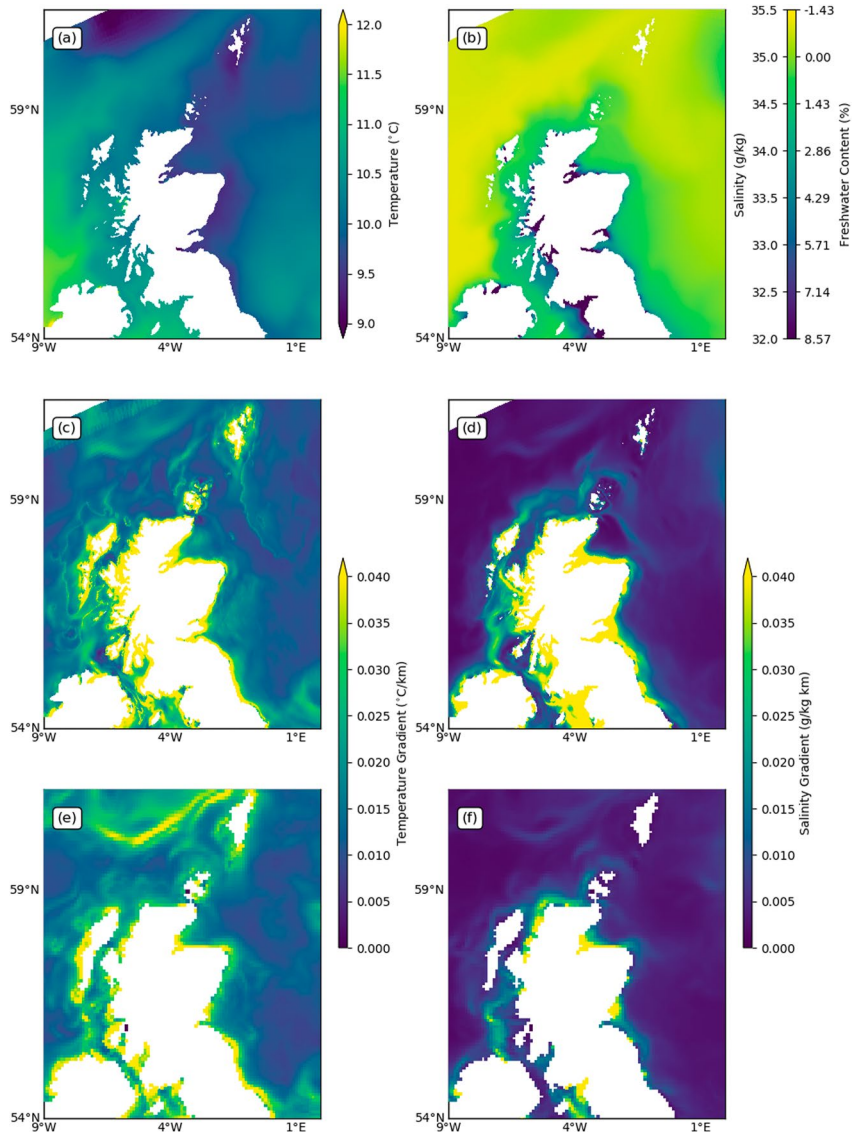

Figure 5. (a) Scottish Shelf Water-Reanalysis Service (SSW-RS) surface temperature averaged over 1993–2019. (b) Same as (a) but for salinity and freshwater content relative to 35 g/kg. (c) SSW-RS surface temperature gradient magnitude averaged over 1993–2019 (note, not the gradient of (a)). (d) Same as (c) but for salinity. (e) Atlantic Margin Model 7 km (AMM7) surface temperature gradient magnitude averaged over 1993–2019. (f) Same as (e) but for AMM7 salinity.

These persistent salinity fronts are features that are absent from AMM7 (Figure 5f). The bias toward more saline coastal surface water in AMM7 has previously been identified (O'Dea et al., 2017). AMM7 is forced with climatology river forcing. It is likely the coarser coastal resolution in AMM7 that prevents the coastal freshwater system from developing into a coherent feature.

We now return to the question of what controls these salinity fronts. The main criteria for a surface-trapped plume in the simplest form is the ratio W_w/W_α (Lentz & Helfrich, 2002). Here, W_α is the distance between the coast and the point at which the plume separates from the bottom, W_w is the distance from the plume bottom separation point to the offshore surface edge of the plume. When $W_w/W_\alpha < 1$, the plume is surface-trapped. When $W_w/W_\alpha \geq 1$, the plume is slope-controlled. To estimate this ratio we need the surface expression of the front and the bottom expression of the front. The surface expression of the offshore salinity front is taken as the 35 g/kg contour (Figure 6). Here, we define the bottom separation point as the 50% contour for the frequency that the (top-bottom) density difference is >-0.01 kg/m^3 (Figure 6b). This is supported by the mean top-bottom density difference. Where the bottom separation point is closer to the surface expression than the coast, the

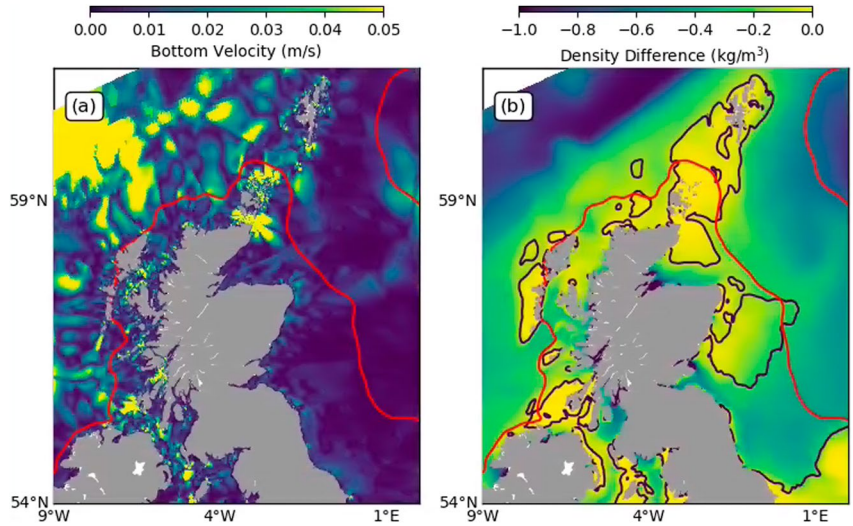

Figure 6. (a) The absolute bottom current speed perpendicular to the nearest coastline (including islands) averaged over the full time period 1993 to 2019. (b) The vertical (top-bottom) density difference averaged over the full time period 1993 to 2019. The red contour in (a) and (b) is the 35 g/kg mean surface salinity contour which is a proxy for the location of the salinity front. The dark blue contour in (b) is the 50% contour for the frequency that the (top-bottom) density difference is >-0.01 kg/m^3.

plume can be classes as slope-controlled and where the bottom separation point is closer to the coast then the surface expression, the plume can be classed as surface-trapped. This identifies the north west coast of Scotland as having a surface-trapped salinity front and the north east coast of Scotland (east of Orkney) as having a slope-controlled salinity front. This is in agreement with vertical salinity gradients present west of Scotland (Hill et al., 1997; Inall et al., 2009), and the lack of vertical salinity gradient in the near coastal part of the JONSIS line (Sheehan et al., 2017).

To support these conclusions, Chapman and Lentz (1994) suggests the criteria for slope-controlled plumes is bottom velocity directed away from the coast up to the front, at which point the bottom velocity should go to zero at the front. Figure 6a shows the component of the bottom currents flowing perpendicular to the nearest coastline. On the north east coast, the bottom velocities are close to zero around the bottom separation point and smaller than on the north east coast.

3.3. Salinity Front Variability

In this section, we will investigate the temporal variability in the coastal freshwater and use a momentum balance to understand the dynamics of the front. Since the water in the coastal region is not temperature stratified (not shown), we focus on surface salinity.

To break down the temporal variability in the coastal freshwater, four transects are used (Figure 1b). The transects show there is some interannual variability and weekly to monthly variability in both the distance of the freshwater away from the coast and the salinity of the freshwater region (Figures 7a–7d, right panels). Transects 1 and 2 appear to have coastal freshwater within 80 km of the coast but Transects 3 and 4 have times when freshwater appears to advect >100 km away from the coast. This is especially true for Transect 4, the most easterly transect. The residual current speed along each transect shows above average transport at the salinity fronts around 50 km offshore for Transect 1 and 2, this is the Atlantic Inflow Current (see Figure 1b) that flows west of the Outer Hebrides (Jones et al., 2020; Porter et al., 2018) (Figures 7a and 7b, left panels). A larger peak residual current speed exists between 120 and 150 km offshore in Transect 1 and 2, this is associated with the shelf break 200 m bathymetry contour. There is some residual current speed within 20 km of the coast that passes east of the Outer Hebrides (see Figure 1b), the Scottish Coastal Current (Hill et al., 1997; Inall et al., 2009). The Atlantic Inflow Current and Scottish Coastal Current are each associated with maintaining the salinity fronts. For Transects 3 and 4, the residual current speed is weaker, as expected given the weaker frontal salinity gradient than

10.1029/2023EA002872

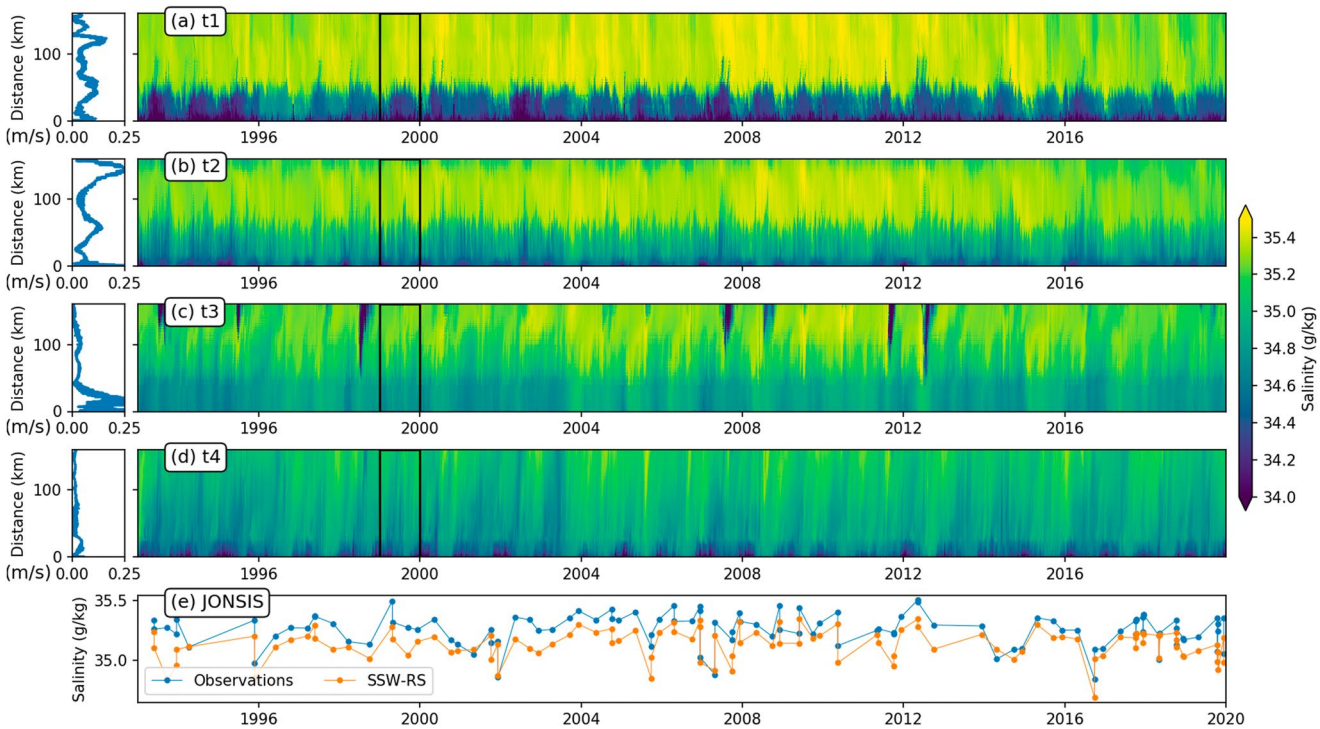

Figure 7. (a–d) Left panels show residual current speed for the respective transects at the locations shown in Figure 1. (a–d) Right panels show surface salinity transects plotted against distance from the coast and time at the locations shown in Figure 1. From (a–d), transects are located t1–t4, clockwise from west to east of Scotland. Each transect extents at least 150 km from the coast with relative distance shown on the transect map. The model points are averaged into 100 m bins and selected in a width of 15 km along the transect line. Black box, highlights time period shown in Figure 8. (e) Joint North Sea Information System (JONSIS) line salinity for observations and Scottish Shelf Water-Reanalysis Service. JONSIS line data are averaged spatially to produce the time series of surface salinity.

Transects 1 and 2 (Figures 7c and 7d, left panels). The residual current speed at 50 km from the coast shows no peak in Transects 3 and 4, however, there is a small peak within 20 km of the coast.

To be sure that the variability in coastal salinity is not an artifact in the model, a comparison can be made with the JONSIS line, a long term observation transect east of the Orkney Isles (Figure 1b). The episodes of CW and AW carried in the Fair Isle Current or East Shetland Current (a continuation of the Atlantic Inflow Current) are found in the JONSIS line (see Figure 1b) (Sheehan et al., 2020). The transport through this section is maintained by the year-round salinity gradient and associated Scottish Coastal Current (Sheehan et al., 2017). Surface salinity in SSW-RS has a −0.1 g/kg salinity bias under the JONSIS line observations (Figure 7e). The fresher model values may be the result of the boundary conditions, an imbalance in the supply of freshwater to salty AW. Both the observations and SSW-RS show a salinity front around 1.5°W so the frontal location is not the source of the bias (not shown). There is consistent variability in the salinity between SSW-RS and the observations, for example, a fresher time period in 2001 and after 2014. These fresh periods suggest the model is correctly simulating the interannual variability in freshwater advecting away from the coast. Note that the salinity in the JONSIS line has temporal aliasing of the higher frequency variability, for example, see Transect 3 (Figure 7).

The low salinity spikes entering from offshore in Figure 7c are recirculation events of freshwater from the Baltic Sea outflow that runs along Norway (not shown). They should be present at the location of the JONSIS line but have mostly been unresolved due to the intermittent and short time frame of the spikes which only last a month or two. The low salinity spike in 2007 shows some signature in the JONSIS line and the event appears stronger in the observations than the model (Figure 7e). The spikes are not present in Transect 4 because Transect 4 aligns with the Dooley current rather than crossing it.

One year is selected to show the high temporal variability. Over 1999, a clearer picture of the short term variability emerges (Figure 8a). In Transect 1 the salinity gradient is a step change from 34.4 to 35.4 g/kg. There is evidence that for periods up to a week, fresher water <34 g/kg of salinity is present close to the coast, for example, May 1999 in Figure 8a(t1). The CW to AW (salinity 34.5–35 g/kg) front shifts between 30 km offshore in

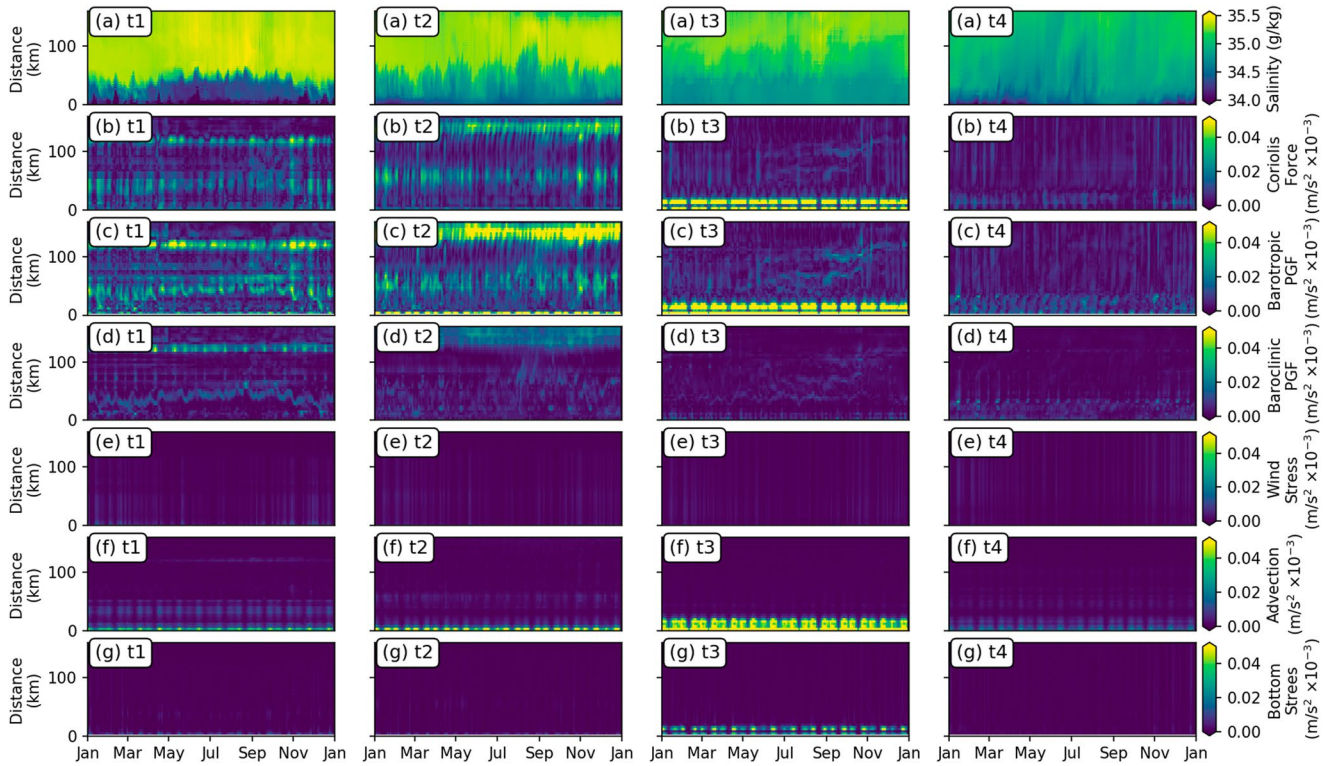

Figure 8. (a) Shows surface salinity transects plotted against distance from the coast and time at the locations of the transects t1, t2, t3, and t4 shown in Figure 1. This is plotted for a 1 year time period to show the short time scale variability for example, year 1999. The momentum balance processes for the transects (t1–t4) are shown in (b)–(f). (b) Show depth integrated Coriolis force component of the momentum balance for each of the transects. (c) Show the barotropic based pressure gradient force (PGF) for each of the transects. (d) Show the baroclinic PGF for each of the transects. (e) Show the wind stress component for each of the transects. (f) Show the advection of momentum component for each of the transects. (g) Show the bottom stress component for each of the transects. Each plot is for a 1 year time period to show the short time scale variability for example, year 1999. The momentum components are filtered with a 3 day running mean and show the magnitude of the *u* and *v* components.

February 1999 to 70 km offshore in August 1999. Figure 7 suggests some of this shifting in salinity in Transect 1 may be seasonal. Figures 8b–8g(t1) show the major components of the momentum balance in Transect 1. The CW to AW front is a balance of acceleration from 0.04×10^{-3} ms^{-2} Coriolis force, 0.05×10^{-3} ms^{-2} barotropic, 0.02×10^{-3} ms^{-2} baroclinic PGF, $<0.01 \times 10^{-3}$ ms^{-2} wind stress, 0.01×10^{-3} ms^{-2} advection of momentum and $<0.01 \times 10^{-3}$ ms^{-2} bottom stress. This shows the contribution to momentum from the baroclinic PGF (i.e., the density gradient between the watermasses) is about half the strength of the barotropic PGF (i.e., surface slope contribution). The front is in geostrophic balance.

Transect 2 has more daily variability than Transect 1, likely a result of tidal currents (Figure 8a(t2)). The front in Transect 2 has a gradient from 34.6 to 35.4 g/kg and varies between 40 and 100 km offshore. The CW here is saltier (freshwater is more mixed/dilute) than in Transect 1. The daily variability introduces more saline water into the coastal freshwater. Figure 6a showed strong bottom velocity in this region north of Scotland, which shows mixing is taking place here. There are times when low salinity water is clearly moving away from the coast, late April 1999 and early August 1999 are some examples (Figure 8a(t2)). Beyond the daily variability, there is weekly to monthly variability that is similar to Transect 1. Transect 2 shows the momentum for the CW to AW front is a balance of 0.05×10^{-3} ms^{-2} Coriolis force, 0.05×10^{-3} ms^{-2} barotropic with a 0.02×10^{-3} ms^{-2} contribution from the baroclinic PGF and little stress or advection (Figures 8b–8g(t2)). The magnitude of the acceleration at Transect 2 is similar to Transect 1 but baroclinic and barotropic pressure force have a peak where the geostrophic balance is interrupted and the low salinity water is moving away from the coast in August 1999.

East of the Orkney Islands, in Transect 3, the front has a weak structure (Figure 8a(t3)). The salinity gradient is 34.7–35.3 g/kg so we do not have water which fully fits the CW definition, it has been mixed too much. The front varies between 50 and 100 km distance offshore. Most of the variability here is on the timescale of weeks to months. Transect 3 has more regular freshwater advecting away from the coast than in Transect 2, making water >100 km offshore less saline. The advection is shown by the diagonal low salinity patches in the figure moving away from the coast over time. The drift speed away from the coast of the low salinity patches is between 1.5 and 3 km/day (estimated from Figure 8a(t3)). These diagonal patches are periodically replaced by high salinity AW. The AW does not show signs of drift shore-wards from offshore in the surface salinity data (Figure 8a(t3)), meaning it must be rapidly advecting shore-wards or it is upwelling from below the surface. Figure 6b shows the outer part of Transect 3 has a vertical density gradient. Figures 8b–8g(t3) shows the momentum at the 50–100 km front in Transect 3 is weaker than Transects 1 and 2 but there is still a contribution from 0.02×10^{-3} ms^{-2} Coriolis force, 0.03×10^{-3} ms^{-2} barotropic and 0.02×10^{-3} ms^{-2} baroclinic PGF so the relative strength of Coriolis force is weakened compared to the barotropic and baroclinic PGF. The freshwater drifts offshore more easily here because it is less inhibited by Coriolis force. Within 30 km of the coast, there is strong acceleration $>0.07 \times 10^{-3}$ ms^{-2} for Coriolis force and barotropic PGF. There is no effect of the salinity front here as shown by the low baroclinic PGF at 0.01×10^{-3} ms^{-2} but there is $> 0.03 \times 10^{-3}$ ms^{-2} contribution to momentum both from bottom stress and advection of momentum. The strong stress and advection here is an indication of the strong tidal currents, enhancing bottom stress from water passing through the Pentland Firth between Orkney and the mainland.

In the most easterly transect, Transect 4, there is no persistent front but there is intermittent CW within 40 km of the coast. (Figure 8a(t4)). Instead, the freshwater advects away from the coast, seen as diagonal lines in the figure. This is because the transect lies along the Dooley Current (see Figure 1b) (Mathis et al., 2015), which will be discussed more in Section 4. The weekly to monthly variability here again seems to follow the variability in Transects 2 and 3, generally showing more advection away from the coast in March and May 1999 while less in late August 1999. The longer term variability is a feature that requires further analysis to understand and is addressed in the next section. Figures 8b–8g(t4) show Transect 4 has much lower acceleration than in Transects 1, 2 and 3. In Transect 4, momentum is largest within 40 km of the coast with around 0.02×10^{-3} ms^{-2} Coriolis force, 0.03×10^{-3} ms^{-2} barotropic, 0.02×10^{-3} ms^{-2} baroclinic PGF, $<0.01 \times 10^{-3}$ ms^{-2} wind stress, 0.02×10^{-3} ms^{-2} advection and $<0.01 \times 10^{-3}$ ms^{-2} bottom stress.

3.4. Salinity Interannual Variability

To better understand the sources of freshwater to the sea around Scotland, we calculated a freshwater budget for the black box in Figure 1a. The freshwater budget shows the surface flux is negative when averaged over a year (i.e., more evaporation than precipitation) (black line in Figure 9a). The 27-year temporal mean total surface flux is −1,520 m^3/s and standard deviation is 331 m^3/s. The temporal mean total river freshwater flux is 3,150 m^3/s and standard deviation is 386 m^3/s. The temporal mean total boundary freshwater flux is −662 m^3/s and standard deviation is 8910 m^3/s. For completeness, the mean freshwater volume change is 964 m^3/s and standard deviation is 9020 m^3/s. The river flux provides the source for the majority of the mean freshwater exported from the region, however its interannual variability is smaller than the variability in boundary transport. The freshwater transport and freshwater volume change have similar interannual variability. The interannual variability in total surface freshwater flux and river flux are low in comparison.

To deconstruct the interannual variability of surface salinity around Scotland, maps of EOFs (EOF), along with timeseries of principal components (PC), were calculated. These were calculated for the same area as the freshwater budget. These EOFs are cohesive modes of variability in salinity and given that we look at a coastal setting, the strongest modes are associated with the ROFI around Scotland. The first mode of variability accounts for 45% of the variability in surface salinity, while the second accounts for 21%. These two modes are the focus of this analysis as the third mode only accounts for 6% of variability, a clear drop in explained variability. EOF1 of surface salinity acts in unison across most of the analysis area (Figure 10). The reader should interpret the EOFs by looking at both the EOF map pattern and the associated PC time series together in a multiplicative sense which gives the response in the number of salinity standard deviations at a chosen time. For example, EOF1 has a large negative center, so times when the associated PC1 time series is increasing would be interpreted as the map center having a decreasing salinity signal. The strongest response to EOF1 is within the region of coastal freshwater

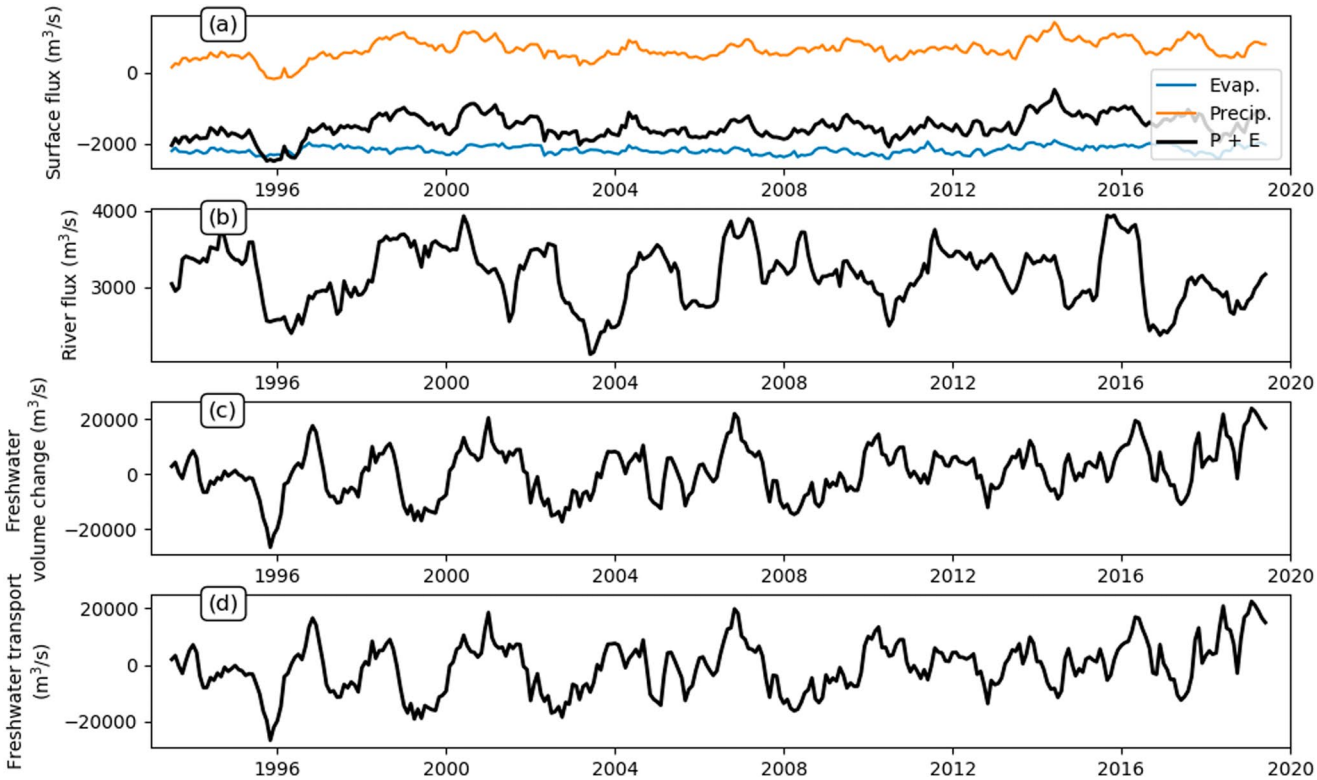

Figure 9. Freshwater budget for the box used in the empirical orthogonal function analysis (54°N to 61°N and 10°W to 2°E, Figure 1b). The components of the budget shown are (a) the total precipitation plus evaporation (F_{surf}), the evaporation, the precipitation, (b) total river flux(F_{riv}), (c) total freshwater volume change (F_{vol}) relative to $S = 35$ g/kg, (d) total oceanic freshwater transport (F_{tr}) relative to $S = 35$ g/kg. Note, all positive values show a flux into the box.

(Figure 5). Empirical orthogonal functions usually have a dipole pattern but for EOF1 we only see one pole, this is because the second pole will be outside the analysis box, likely to the south. PC1 combined with EOF1 shows positive salinity anomalies (negative PC1) around Scotland in 1996, 2004, 2008, 2010, and 2015 (Figure 10c). There are also negative salinity anomaly around Scotland in 1993–1994, 2002, 2007, 2012, and 2016.

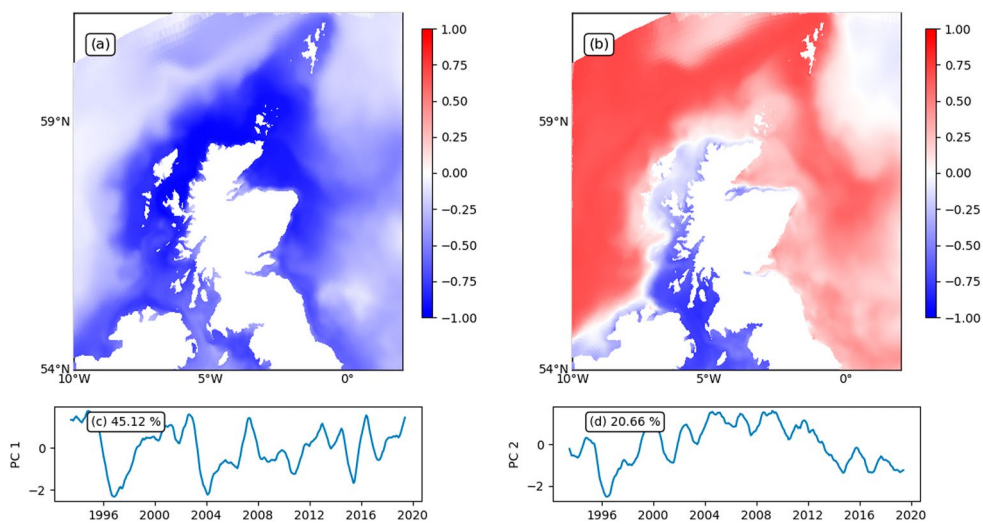

Figure 10. Empirical orthogonal function analysis of surface salinity with 12 month running mean. The analysis region selected is 54°N to 61°N and 10°W to 2°E, Figure 1b. (a) EOF1 spatial pattern, (b) EOF2 spatial pattern. (c) The timeseries of PC1 associated with EOF1. (d) The timeseries of PC2 associated with EOF2. Given that the salinity is pre-processed by dividing by the standard deviation the units are number of standard deviations.

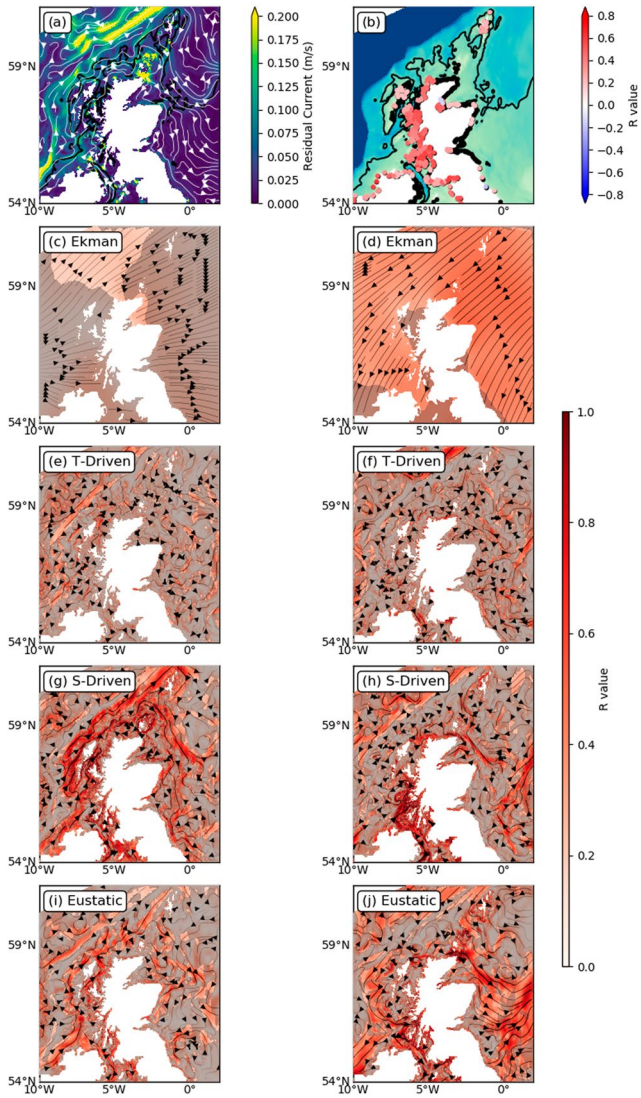

Figure 11. (a) Residual current speed calculated by mean over 1993–2019. White arrows show the current stream direction. Black contour marks the 100 m isobath. (b) Regression value of river volume flux with principal component 2 (see Figure 10d). Background colormap shows Scottish Shelf Water-Reanalysis Service bathymetry as in Figure 1. Red points are in-phase with PC2, blue points are out of phase. Black points are insignificant regression values. (c–j) Regression value of depth averaged *u* and *v* current components from various energy sources with principal components (PC) 1 and 2 (see Figures 10c and 10d). (c, d) Depth averaged *Ekman* current against PC1 and PC2 respectively. (e, f) Depth averaged *T-Driven* current against PC1 and PC2 respectively. (g, h) Depth averaged *S-Driven* current against PC1 and PC2 respectively. (i, j) *Eustatic* current against PC1 and PC2 respectively. Red areas and directional arrows are in-phase with the PC, gray areas show insignificant regression values. When interpreting the regressions during the negative PC anomaly the color map will be the same but the directional arrows will reverse.

The mean residual current around Scotland flows from Ireland clockwise around the west, north and east coast of Scotland (Figure 11a). One band of stronger current flows closer to the coast and east of the Hebrides (the Scottish Coastal Current see Figure 1b (Inall et al., 2009)), while another branch flows further offshore west and north of the Hebrides (the Atlantic Inflow Current see Figure 1b (Jones et al., 2020; Porter et al., 2018)). Although we previous found the residual currents are mostly driven by the barotropic forcing (the largest source of acceleration in Figure 8), for the EOF analysis we are interested specifically in variability. Next we regress PC1 against currents, the strength of the regression with each *u* and *v* component are combined to indicate what direction of transport the EOF is responding to. Regression of PC1 with the Ekman transport velocity components shows mostly insignificant regression values (Figure 11c). There is only a small portion north of Scotland that has significant but low regression values <0.25. PC1 has a regression value of 0.33 with the 12-month running mean of the North Atlantic Oscillation index supporting the idea that wind stress variability has a minimal effect on PC1. The EOFs are unlikely to be correlated with the south eastward Ekman transport (south westerly prevailing winds) because the EOF is looking at modes of variability that is, deviations from the prevailing conditions. The regression of PC1 with the *S-Driven* velocity shows values >0.7 along the 35 g/kg offshore salinity front (Figure 11e). There is also a region east of Scotland that shows significant regression >0.6, suggesting a northward shift and strengthening in the Dooley Current during an EOF1 negative salinity anomaly. As expected, the regression of PC1 with the *T-Driven* velocity is almost entirely insignificant. Regression of PC1 with the *Eustatic* velocity shows values >0.5 along the 35 g/kg offshore salinity front to the west of Scotland but this reduces to <0.4 east of Scotland (Figure 11g). Given that the regression for the *Eustatic* velocity is weaker than the *S-Driven* velocity, the *Eustatic* regression values are due to the variability in the river volume flux, which would be in phase with the salinity, as it cannot be the salinity itself. Total river flux within the box (Figure 9c) is correlated with PC1 with *r*-value 0.39, again this is low because the salinity in EOF1 is mainly influenced by advection of freshwater from remote rivers around the British Isles. Regressions of PC1 with precipitation plus evaporation are insignificant (not shown).

The regressions show variability in *S-driven* currents are a stronger forcing factor on PC1 than wind or large-scale variability. This shows anomalously stronger current speed around Scotland occur with the EOF1 fresh anomaly pattern around the north of Scotland, advecting more freshwater to the region from the ROFI in the Irish Sea and from the west of Ireland. EOF1 should be interpreted as advection and diffusion of freshwater north of Scotland during the negative and positive EOF1 anomalies respectively (Figure 10a). During an EOF1 low salinity anomaly (positive amplitude), the freshwater budget shows the largest source of freshwater in EOF1 is the freshwater boundary transport, which makes up the majority of the freshwater volume variability (Figure 9). Greater river flux can contribute to this anomaly but it is more minor given the low regression value. The pattern in current speed regression values show two freshwater export routes, one north of Shetland (the East Shetland Current see Figure 1b) and one east of Orkney (the Fair Isle Current and Dooley Current see Figures 1b and 11c) (Mathis et al., 2015). During an EOF1 high salinity anomaly (negative amplitude), there would be weaker a *S-Driven* current and cross-shelf AW advection/diffusion would tend to increase salinity as shown by Figure 9.

The second mode in surface salinity, EOF2 is a dipole between the coast of Scotland and salinity offshore of 30 km (Figure 10b). The coastal part of this dipole is concentrated on the west coast of Scotland and Northern

Ireland. The spatial pattern in EOF2 closely resembles the 35 g/kg salinity front on the west of Scotland where the front is surface-trapped. PC2 combined with EOF2 has positive coastal salinity anomalies in 1999, 2002, 2004–2009 and 2011 (Figure 10d). There are also negative coastal salinity anomalies in 1996, 2001 and 2013–2018.

PC2 shows positive regression values with interannual variability in river volume flux (Figure 11b). The regression values are >0.4 for the majority of rivers in north and west Scotland (Figure 11b). This is a collective pattern of freshwater import over a year in this region rather than an individual river source. Regression of PC2 with the *Ekman* transport velocity components shows significant regression values over the region with values >0.5 (Figure 11d). The regression is strongest with south-westward *Ekman* transport that is, north-westerly winds. Regression of PC2 with *T-Driven* velocity is mostly insignificant. The regression of PC2 with the *S-Driven* velocity is strongest within 20 km of the coast to the west and north of Scotland where values are >0.8 (Figure 11f). This *S-Driven* current aligns with the zero amplitude response in EOF2 showing this mode in salinity tends to enhance this density gradient across the near coast portion of the front. The *S-Driven* current regression values show a stronger southerly part of the Dooley Current than the regression of PC1 against *S-Driven* currents Figures 11e and 11f. The regression of PC2 with the *Eustatic* velocity has values >0.6 across large parts of the region (Figure 11h). The key feature here is that the regression with currents west of Scotland are directed south-westward and the regression with currents east of Scotland are directed south-eastward, that is, a divergence.

The second mode of surface salinity is primarily wind driven variability. Although the *Ekman* regression is not the strongest, it supports the strong *Eustatic* and *S-Driven* regression values. During an EOF2 positive amplitude anomaly, the *Ekman* currents push water south-westward toward north east of Scotland where the landmass acts as a wedge dividing the flow either side. This can be seen in the *Eustatic* currents where the *Ekman* currents would tend to push water toward the coast and increase the surface elevation gradient (stronger *Eustatic* currents) on the east coast of Scotland and tend to push water away from the west coast decreasing the surface elevation gradient (weaker *Eustatic* currents). The divergence around the north east of Scotland and the concurrent south westward currents along the shelf break will draw saline AW from the opposing slope current and Atlantic Inflow Current onto the shelf to balance the divergent transport. Some variability in transport in the currents east of Shetland have been linked to wind stress (Hughes, 2013). The drawing of AW onto the shelf explains the saline anomaly in EOF2 and the stronger Dooley Current will influence the North Sea with a saline anomaly (Figure 10b). A fresh salinity anomaly to the west of Scotland occurs due to the reduced advection of freshwater away from this region and supplemented by stronger river flux (a result of the north-westerly winds). The *S-Driven* coastal current is then intensified closer to the coast. During an EOF2 negative amplitude anomaly, south-easterly winds and north-westward *Ekman* currents will strengthen the export of freshwater from the near coastal area and the negative coastal salinity anomaly will be amplified by the effect of reduced river flux. The convergence around Shetland and the north-westward *Ekman* currents will tend to reduce the cross shelf transport of saline AW.

To summarize, 45% of the variability in salinity comes from the temporal interplay between the high salinity Atlantic Inflow Current and the lower salinity CW ROFI that gives EOF1 strength around Scotland. This occurs all around Scotland with decreasing efficiency away from the coastal ROFI. An additional 21% of variability comes from the *Ekman* transport which acts to modulate when low salinity CW is retained near the west coast of Scotland and when saline AW is draw into the shelf.

4. Discussion

We now return to the question posed in Section 1, is freshwater retained around Scotland and what affects its variability? There appears to be a two mode system of salinity fronts in the coastal freshwater trap around Scotland so we will address each mode individually.

A coastal freshwater front is sometimes referred to as a ROFI or river plume and may be salinity stratified (Simpson, 1997). This is different to the tidal mixing fronts described around the UK by Holt and Umlauf (2008). The freshwater region between the coast and the 50–80 km offshore CW to AW front is clearly a ROFI but it can also be classified as surface-trapped or slope-controlled according to the ratio W_w/W_α (Lentz & Helfrich, 2002). The ROFI around Scotland is a surface-trapped plume north of 56°N and west of 3°W, while east of 3°W the ROFI behaves more like a slope-controlled plume (Figure 6). The controlling dynamics are the constraint of Coriolis and the PGF which is itself supported by the density gradient. The density gradient is maintained by the renewal of riverine freshwater, advected freshwater and advected saline water (Figure 9). To answer the first part of our question, freshwater is retained to the west and north of Scotland where there is a geostrophic front. This

retention degrades in the North Sea, where the AW to CW front is poorly defined but the influence of temporal variability in salinity in the western front is found in the east.

The west-east difference in the strength of frontal gradient is a result of the changes in the geostrophic balance which are influenced by bathymetry and dynamical processes introduced by the presence of the Orkney Isles. There are documented cases of currents stabilized by topography losing their stability when they cross bathymetric obstacles (Rintoul, 2018). This tends to increase the formation of eddies which allow stirring and mixing of water across fronts (Thompson & Garabato, 2014). In the case of our front, the Orkney Isles produces strong tidal currents (De Dominicis et al., 2017). This results in the advection of momentum (see in Figure 8f(t3)) and the mixing of AW with CW, eroding the salinity gradient. Further south at the Dooley Current which runs along the 100 m isobath (Mathis et al., 2015), the currents diverge from the coast carrying freshwater away. This prevents the front from re-forming to the south.

To answer the second part of our question we focus on interannual variability. There are several aspects to temporal variability that are also spatially variable. The primary mode of variability in freshwater is caused by a change in the supply of freshwater. The currents cause the convergent concentration of freshwater north of Scotland while moving the salinity front further offshore to accommodate the freshwater storage, for example, 2007 as seen in Figure 7 and the freshwater volume change in Figure 9. When the freshwater supply is enhanced the salinity of the CW decreases more than the offshore salinity, as shown by EOF1. Equally, the freshwater in this area can become more concentrated with salt when the coastal current is reduced. This will not only affect the gradient of the front but also the advection of freshwater along it and the salinity variability beyond the front into the North Sea via circulation around the Orkney Islands, which we will refer to as Pathway 1. This flips every 1–3 years between concentration and dilution with a weak influence (r-value = 0.33) from North Atlantic Oscillation.

The east-west difference associated with the front between AW and CW is captured by EOF2 (Figure 10b). This can be most clearly seen in the location of the divide between positive and negative spatial patterns in EOF2 which lines up with the mean salinity front in the west (Figures 10b and 5d). This agrees with our regression that the positive and negative spatial pattern on Figure 10b are an *Ekman* driven interplay in mixing between Atlantic Inflow Water influence and river flux influence. In the positive anomaly, freshwater is retained shore-ward of the front while a stronger East Shetland Current and southern Dooley Current advects saline AW into the North Sea. During the negative anomaly, freshwater is advected through the boundary from the current northwest of Ireland (Irish CW) and northward out of the Irish Sea, making the Atlantic Inflow current fresher (red region in Figure 10b) and the coastal area saltier. The freshwater anomaly can propagate into the North Sea via the Shetland Islands (and East Shetland Current) and has a weakened southern Dooley Current, Pathway 2 (Figures 10 and 11b). This second path has mostly occurred 1996–1999 and 2013–2019. The switch to this second pathway is not mutually exclusive to Pathway 1. This route is influenced by the wind and the associated *Ekman* transport which either blocks Pathway 2 to coastal freshwater or promotes it with the leakage of freshwater away from the coast into the Atlantic Inflow Current.

To summarize, given that EOF1 accounts for a larger percentage of variability than EOF2, it suggests the advection diffusion process is more responsible for the variability in surface salinity and the timing of freshwater anomalies that ultimately escape the coastal area through the Dooley Current. The advection away from the coast is periodically enhanced but is also a gradual process along the mean transport route from west to east of Scotland but mostly occurring east of Orkney.

5. Conclusion

In this analysis we developed the SSW-RS, an unstructured-grid model with dynamic resolution down to 500 m at the coast, enabling it to resolve coastal processes. The simulation benefits from a high resolution river data set with daily variability, SST assimilation, tides, boundary ocean forcing and atmospheric forcing. Comparison of SSW-RS output with in situ hydrographic profiles shows SSW-RS captures seasonal spatial patterns, watermasses and temporal variability in temperature and salinity. SSW-RS is able to resolve fresh CW dynamics that are missed by the coarser coastal resolution in the 7 km Northwest European Shelf NEMO simulation, AMM7. It has been largely acceptable to have relatively few river discharge points and climatology river forcing in ocean models until now but we show that improved spatial and temporal river resolution has a strong impact on coastal dynamics and freshwater flux away from the coast.

We take advantage of the coastal freshwater resolution to analyze the spatial and temporal variability in surface salinity around Scotland. We focus on a salinity front between AW and CW which sits 50–80 km from the coast. The offshore front is a persistent feature west and north of Scotland but breaks down east of the Orkney Isles

allowing freshwater to flow away from the coast in the East Shetland Current and Dooley Current. Empirical orthogonal function analysis shows variability in the location and salinity of the offshore front is captured by EOF1 and EOF2, making up 66% of the variability in surface salinity. The first mode is correlated with the *S-Driven* variability in the Scottish Coastal Current and Atlantic Inflow Current that supports periodic concentration of freshwater north of Scotland and advective dilution. The second mode is correlated with wind driven *Ekman* transport which can promote anomalous cross shelf transport of saline water which propagates into the North Sea and concentrates freshwater west of Scotland. The other side of this mode is the diffusion of freshwater into the Atlantic Inflow Current and away from the coast.

The location and temporal variability in the freshwater fronts around Scotland are important because the fronts can contain or release freshwater, nutrients, pollutants or planktonic larvae in the coastal region, potentially affecting grazing locations and habits of fish. The concentration and dilution of the freshwater will affect the density, the currents and contributes to seasonal stratification of the North Sea.

Appendix A: Additional Validation Figures

This appendix contains the additional validation carried out for temperature and salinity of SSW-RS and AMM7 against observation profiles (Figure A1). Comparisons are also made between SSW-RS and AMM15 in the overlap year of 2019 against observations profiles (Figure A2).

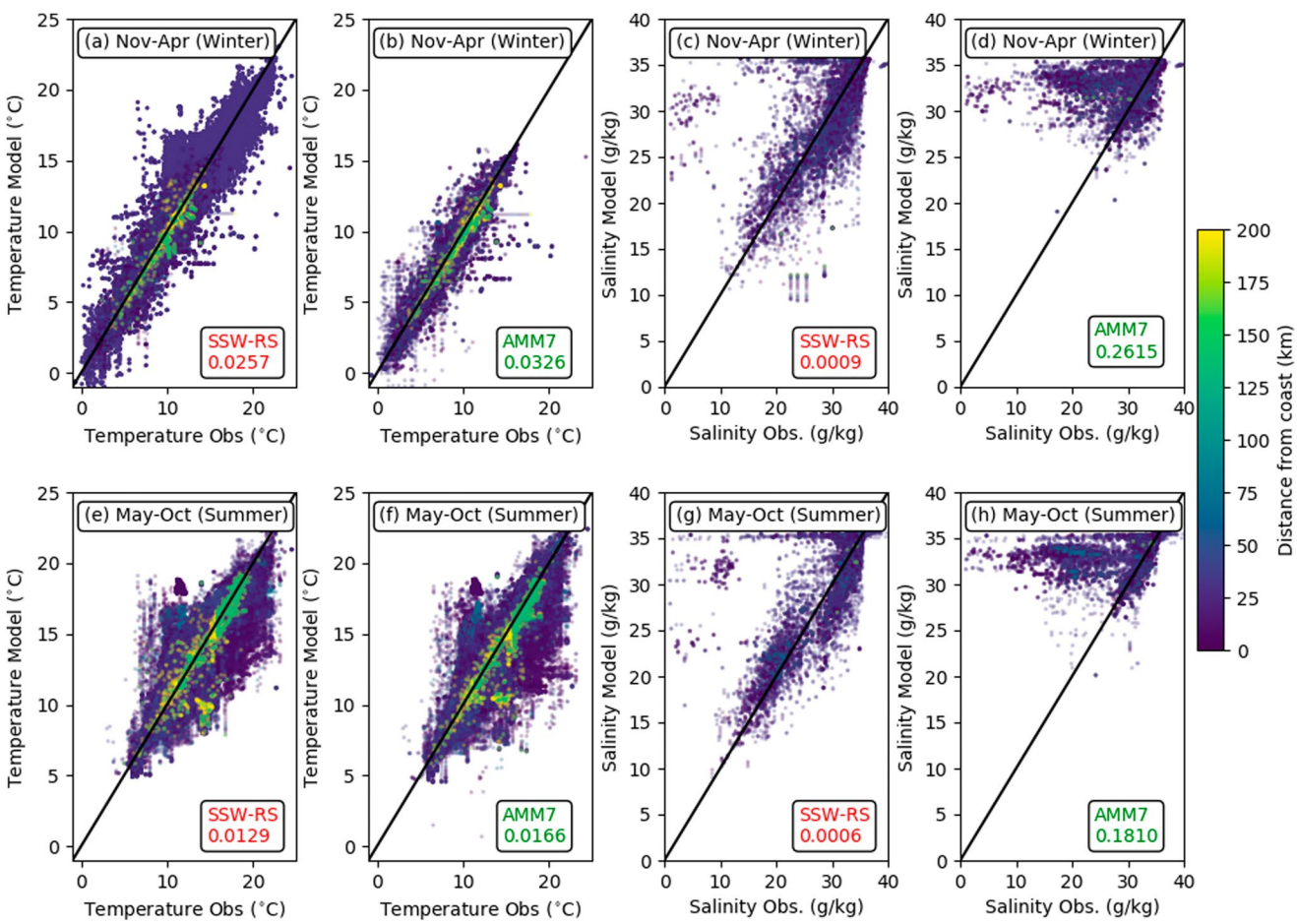

Figure A1. Scatter diagrams of model versus observations for Scottish Shelf Water-Reanalysis Service (SSW-RS) and Atlantic Margin Model 7 km. (a), (b), (e), (f) Temperature and (c), (d), (g), (h) salinity. (a), (b), (c), (d) Show November-April and (e), (f), (g), (h) show May-October, which we refer to as winter and summer respectively. Black line is 1-to-1 line. In each figure, the respective root mean square error is shown in bottom right (for temperature units are °C and salinity units are g/kg). 897,745 temperature points and 210,954 salinity points were used. Data are shown for profiles on the shelf in depth <200 for the whole SSW-RS domain.

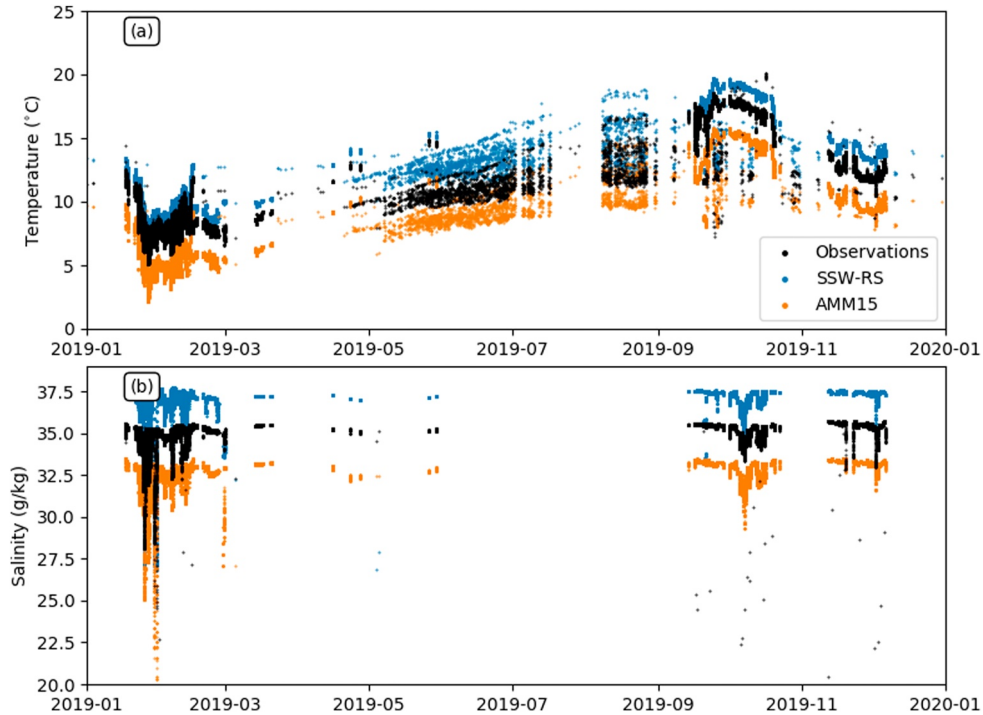

Figure A2. A timeseries of depth averaged profiles in the Scottish Shelf Water-Reanalysis Service (SSW-RS) domain over 2019. (a) Shows temperature and (b) shows salinity. To help with visibility of the data sets, the SSW-RS data in these plots has had an offset deliberately applied of +2°C and +2 g/kg. Similarly the AMM15 data have had a −2°C and −2 g/kg offset applied. Unfortunately, the salinity profiles are only available in the southern North Sea.

Data Availability Statement

Version 3.02 of the Scottish Shelf Water-Reanalysis Service (SSW-RS) based on the UK-FVCOM4.0 model which was used for all analysis, has all model output preserved at https://doi.org/10.7489/12423-1, available via Open access with registration.

Version TPXO9-Atlas of TPXO sea surface height and velocity harmonics used for boundary forcing were downloaded from https://www.tpxo.net/global/tpxo9-atlas, available via Open access with registration.

Issue 1.2 (version 4) of the Atlantic Margin Model 7km with product ID NWSHELF_MULTIYEAR_PHY_004_009, used for boundary forcing, initialization and comparison were downloaded from Copernicus Marine Services via https://doi.org/10.48670/moi-00059, available via Open access with registration.

Issue 2 of the Baltic Sea Physical Reanalysis model with product ID BALTICSEA_REANALYSIS_PHY_003_011, used for boundary forcing and initialization were downloaded from Copernicus Marine Services via https://doi.org/10.48670/moi-00013, available via Open access with registration.

Version ERA5 of ECMWF atmospheric reanalysis data, used for surface forcing were downloaded from ECMWF via https://doi.org/10.24381/cds.adbb2d47, available via Open access with registration.

Issue 1.3 of the ODYSSEA satellite sea surface temperature dataset with product ID SST_ATL_SST_L4_REP_OBSERVATIONS_010_026, used for surface sea surface temperature assimilation were downloaded from Copernicus Marine Services via https://doi.org/10.48670/moi-00153, available via Open access with registration.

Version 3 of E-HYPE data, used for river forcing data were downloaded from the Swedish Meteorological and Hydrological Institute (SMHI) via https://hypeweb.smhi.se/, available under Creative Commons Attribution-ShareAlike 4.0 International (CC BY-SA 4.0).

Version 2.2.0 of PyFVCOM software was used for building model forcing files, for post-processing and analysis, this is preserved at https://doi.org/10.5281/zenodo.2671617, available under MIT License and developed openly at GitHub https://github.com/pmlmodelling/pyfvcom.

Code used for data processing, analysis and plotting is preserved at https://doi.org/10.5281/zenodo.8140138, available under GNU Version 3 License on Github at https://github.com/b-barton/SSW-RS_Analysis/.

Issue 1.14 of Coriolis Ocean Dataset for Reanalysis (CORA) with product ID INSITU_GLO_PHY_TS_DISCRETE_MY_013_001 profile dataset, used for validation of the SSW-RS were downloaded from Copernicus Marine Services via https://doi.org/10.17882/46219, available via Open access with registration.

Issue 1.3 of the Atlantic Margin Model 15 km with product ID NORTHWESTSHELF_ANALYSIS_FORECAST_PHY_004_013, used for comparison were downloaded from Copernicus Marine Services via https://doi.org/10.48670/moi-00054, available via Open access with registration.

Observations from the Marine Scotland Science Joint North Sea Information System (JONSIS) Line, used for validation were downloaded from the Scottish Government (Marine Scotland Directorate) https://marine.gov.scot/information/jonsis-line, available via Open access.

Acknowledgments
This research was funded by Copernicus Marine Environment Monitoring Service under contract code 110-DEM5-L2. Additional support from the NERC INSITE project CHASANS, Grant NE/T010878/1.

References

AMM15-Team. (2022). Atlantic Margin model 15 km (AMM15), issue 1.3 [Dataset]. NORTHWESTSHELF ANALYSIS FORECAST PHY 004 013. https://doi.org/10.48670/moi-00054

AMM7-Team. (2022). Atlantic Margin model 7km (AMM7), issue 1.2 (version 4) [Dataset]. NWSHELF MULTIYEAR PHY 004 009. https://doi.org/10.48670/moi-00059

Arheimer, B., Pimentel, R., Isberg, K., Crochemore, L., Andersson, J., Hasan, A., & Pineda, L. (2019). Global catchment modelling using World-Wide HYPE (WWH), open data and stepwise parameter estimation. In *Hydrology and Earth system sciences discussions* (pp. 1–34). https://doi.org/10.5194/hess-2019-111

Armitage, T. W. K., Bacon, S., Ridout, A. L., Thomas, S. F., Aksenov, Y., & Wingham, D. J. (2016). Arctic sea surface height variability and change from satellite radar altimetry and GRACE, 2003–2014. *Journal of Geophysical Research: Oceans*, *121*(6), 4303–4322. https://doi.org/10.1002/2015JC011579

Autret, E., Tandéo, P., Paul, F., Prévost, C., & Piollé, J. F. (2019). *Product user manual for level 4 Odyssea reprocessed SST product over the European North West Shelf/Iberia Biscay Irish seas SST_ATL_SST_L4_REP_OBSERVATIONS_010_026 (technical report no. 1.2)*. Ifremer, Brest: Copernicus.

Balls, P. W. (1985). Trace metal fronts in Scottish coastal waters. *Estuarine, Coastal and Shelf Science*, *20*(6), 717–728. https://doi.org/10.1016/0272-7714(85)90028-9

Baltic-Sea-Physical-Reanalysis-Team. (2020). Baltic Sea physical reanalysis, issue 2 [Dataset]. BALTICSEA REANALYSIS PHY 003 011. https://doi.org/10.48670/moi-00013

Barton, B. I. (2023). SSW-RS analysis [Software]. National Oceanography Centre, Liverpool, United Kingdom. https://doi.org/10.5281/zenodo.8140138

Barton, B. I., De Dominicis, M., O'Hara Murray, R., & Campbell, L. (2022). *Scottish shelf model 3.02 – 27 Year reanalysis*. National Oceanography Centre, Liverpool, United Kingdom. https://doi.org/10.7489/12423-1

Barton, B. I., Lenn, Y.-D., & Lique, C. (2018). Observed Atlantification of the Barents Sea Polar Front limits the expansion of winter sea ice. *Journal of Physical Oceanography*, *48*(8), 1849–1866. https://doi.org/10.1175/JPO-D-18-0003.1

Barton, B. I., Lique, C., & Lenn, Y.-D. (2020). Water mass properties derived from satellite observations in the Barents sea. *Journal of Geophysical Research: Oceans*, *125*(8), e2019JC015449. https://doi.org/10.1029/2019JC015449

Bell, V. A., Kay, A. L., Rudd, A. C., & Davies, H. N. (2018). The MaRIUS-G2G datasets: Grid-to-Grid model estimates of flow and soil moisture for Great Britain using observed and climate model driving data. *Geoscience Data Journal*, *5*(2), 63–72. https://doi.org/10.1002/gdj3.55

Bricheno, L. M., Wolf, J. M., & Brown, J. M. (2014). Impacts of high resolution model downscaling in coastal regions. *Continental Shelf Research*, *87*, 7–16. https://doi.org/10.1016/j.csr.2013.11.007

Burchard, H. (2002). *Applied turbulence modelling in marine waters* (p. 100). Springer Science & Business Media.

Cabanes, C., Grouazel, A., Von Schuckmann, K., Hamon, M., Turpin, V., Coatanoan, C., et al. (2013). The CORA dataset: Validation and diagnostics of in-situ ocean temperature and salinity measurements. *Ocean Science*, *9*(1), 1–18. https://doi.org/10.5194/os-9-1-2013

Carmack, E. C. (2007). The alpha/beta ocean distinction: A perspective on freshwater fluxes, convection, nutrients and productivity in high-latitude seas. *Deep-Sea Research Part II Topical Studies in Oceanography*, *54*(23–26), 2578–2598. https://doi.org/10.1016/j.dsr2.2007.08.018

Cazenave, P., & Bedington, M. (2019). PyFVCOM [Software]. Plymouth Marine Laboratory, Plymouth, Devon, United Kingdom. https://doi.org/10.5281/zenodo.8140138

Chapman, D. C., & Lentz, S. J. (1994). Trapping of a coastal density front by the bottom boundary layer. *Journal of Physical Oceanography*, *24*(7), 1464–1479. https://doi.org/10.1175/1520-0485(1994)024%3C1464:TOACDF%3E2.0.CO;2

Chen, C., Liu, H., & Beardsley, R. C. (2003). An unstructured grid, finite-volume, three-dimensional, primitive equations ocean model: Application to coastal ocean and estuaries. *Journal of Atmospheric and Oceanic Technology*, *20*(1), 159–186. https://doi.org/10.1175/1520-0426(2003)020(0159:AUGFVT)2.0.CO;2

de Brye, B., de Brauwere, A., Gourgue, O., Kärnä, T., Lambrechts, J., Comblen, R., & Deleersnijder, E. (2010). A finite-element, multi-scale model of the Scheldt tributaries, river, estuary and ROFI. *Coastal Engineering*, *57*(9), 850–863. https://doi.org/10.1016/j.coastaleng.2010.04.001

De Dominicis, M., O'Hara Murray, R., & Wolf, J. (2017). Multi-scale ocean response to a large tidal stream turbine array. *Renewable Energy*, *114*, 1160–1179. https://doi.org/10.1016/j.renene.2017.07.058

De Dominicis, M., O'Hara Murray, R., Wolf, J., & Gallego, A. (2018). The Scottish shelf model 1990–2014 climatology version 2.01. https://doi.org/10.7489/12037-1

De Dominicis, M., Wolf, J., & O'Hara Murray, R. (2018). Comparative effects of climate change and tidal stream energy extraction in a shelf sea. *Journal of Geophysical Research: Oceans*, *123*(7), 5041–5067. https://doi.org/10.1029/2018JC013832

Egbert, G. D., & Erofeeva, S. Y. (2002). Efficient inverse modeling of barotropic ocean tides. *Journal of Atmospheric and Oceanic Technology*, *19*(2), 183–204. https://doi.org/10.1175/1520-0426(2002)019⟨0183:EIMOBO⟩2.0.CO;2

Egbert, G. D., & Erofeeva, S. Y. (2020). TPXO9-atlas [Dataset]. OSU TPXO Tide Models. Retrieved from https://www.tpxo.net/global/tpxo9-atlas

E-HYPE-Team. (2020). E-HYPE, version 3 [Dataset]. E-Hyper. Retrieved from https://hypeweb.smhi.se/

Fairall, C. W., Bradley, E. F., Rogers, D. P., Edson, J. B., & Young, G. S. (1996). Bulk parameterization of air-sea fluxes for tropical ocean global atmosphere coupled-ocean atmosphere response experiment. *Journal of Geophysical Research C: Oceans*, *101*(C2), 3747–3764. https://doi.org/10.1029/95JC03205

Fong, D. A., & Geyer, W. R. (2002). The alongshore transport of freshwater in a surface-trapped river plume. *Journal of Physical Oceanography*, *32*(3), 957–972. https://doi.org/10.1175/1520-0485(2002)032⟨0957:TATOFI⟩2.0.CO;2

Guihou, K., Polton, J., Harle, J., Wakelin, S., O'Dea, E., & Holt, J. (2018). Kilometric scale modeling of the North West European Shelf Seas: Exploring the spatial and temporal variability of internal tides. *Journal of Geophysical Research: Oceans*, *123*(1), 688–707. https://doi.org/10.1002/2017JC012960

Henry, L. A., Mayorga-Adame, C. G., Fox, A. D., Polton, J. A., Ferris, J. S., McLellan, F., et al. (2018). Ocean sprawl facilitates dispersal and connectivity of protected species. *Scientific Reports*, *8*(1), 1–11. https://doi.org/10.1038/s41598-018-29575-4

Hersbach, H., Bell, B., Berrisford, P., Biavati, G., Horányi, A., Muñoz Sabater, J., et al. (2018). ERA5 hourly data on single levels from 1940 to present [Dataset]. ECMWF. https://doi.org/10.24381/cds.adbb2d47

Hersbach, H., Bell, B., Berrisford, P., Hirahara, S., Horányi, A., Muñoz-Sabater, J., et al. (2020). The ERA5 global reanalysis. *Quarterly Journal of the Royal Meteorological Society*, *146*(730), 1999–2049. https://doi.org/10.1002/qj.3803

Hill, A. E., Horsburgh, K. J., Garvine, R. W., Gillibrand, P. A., Slesser, G., Turrell, W. R., & Adams, R. D. (1997). Observations of a density-driven recirculation of the Scottish coastal current in the Minch. Estuarine. *Coastal and Shelf Science*, *45*(4), 473–484. https://doi.org/10.1006/ecss.1996.0198

Hill, A. E., & Simpson, J. H. (1989). On the interaction of thermal and haline fronts: The Islay front revisited. Estuarine. *Coastal and Shelf Science*, *28*(5), 495–505. https://doi.org/10.1016/0272-7714(89)90025-5

Holt, J., & Proctor, R. (2008). The seasonal circulation and volume transport on the Northwest European continental shelf: A fine-resolution model study. *Journal of Geophysical Research*, *113*(6), 1–20. https://doi.org/10.1029/2006JC004034

Holt, J., & Umlauf, L. (2008). Modelling the tidal mixing fronts and seasonal stratification of the Northwest European Continental shelf. *Continental Shelf Research*, *28*(7), 887–903. https://doi.org/10.1016/j.csr.2008.01.012

Hordoir, R., Axell, L., Höglund, A., Dieterich, C., Fransner, F., Gröger, M., et al. (2019). Nemo-nordic 1.0: A NEMO-based Ocean Model for the Baltic and north seas—Research and operational applications. *Geoscientific Model Development*, *12*(1), 363–386. https://doi.org/10.5194/gmd-12-363-2019

Hughes, S. (2013). *Inflow of Atlantic water to the North sea: Seasonal variability on the East Shetland shelf (unpublished doctoral dissertation)*. University of the Highlands and Islands.

Hurrell, J. W., & Van Loon, H. (1997). Decadal variations in climate associated with the North Atlantic oscillation. *Climatic Change at High Elevation Sites*, *36*(3–4), 301–326. https://doi.org/10.1023/a:1005314315270

Inall, M., Gillibrand, P., Griffiths, C., MacDougal, N., & Blackwell, K. (2009). On the oceanographic variability of the North-West European shelf to the West of Scotland. *Journal of Marine Systems*, *77*(3), 210–226. https://doi.org/10.1016/j.jmarsys.2007.12.012

IOC, SCOR, & IAPSO. (2010). The international thermodynamic equation of seawater – 2010: Calculation and use of thermodynamic properties. Intergovernmental Oceanographic Commission, Manuals and Guides, No. 56(UNESCO). Retrieved from http://www.teos-10.org/.196

Jones, S., Cottier, F., Inall, M., & Griffiths, C. (2018). Decadal variability on the Northwest European continental shelf. *Progress in Oceanography*, *161*(December 2017), 131–151. https://doi.org/10.1016/j.pocean.2018.01.012

Jones, S., Inall, M., Porter, M., Graham, J. A., & Cottier, F. (2020). Storm-driven across-shelf oceanic flows into coastal waters. *Ocean Science*, *16*(2), 389–403. https://doi.org/10.5194/os-16-389-2020

JONSIS-Project. (2021). Joint North Sea Information system (JONSIS) line [Dataset]. JONSIS. Retrieved from https://marine.gov.scot/information/jonsis-line

Larsen, K. M. H., Gonzalez-Pola, C., Fratantoni, P., Beszczynska-Möller, A., & Hughes, S. L. E. (2016). ICES report on ocean climate 2014. *ICES Cooperative Research Report*, *329*, 139.

Lentz, S. J., & Helfrich, K. R. (2002). Buoyant gravity currents along a sloping bottom in a rotating fluid. *Journal of Fluid Mechanics*, *464*, 251–278. https://doi.org/10.1017/S0022112002008868

Levitus, S., Antonov, J. I., Boyer, T. P., Garcia, H. E., & Locarnini, R. A. (2005). Linear trends of zonally averaged thermosteric, halosteric, and total steric sea level for individual ocean basins and the world ocean, (1955–1959)–(1994–1998). *Geophysical Research Letters*, *32*(16), 1–4. https://doi.org/10.1029/2005GL023761

Lewis, H., & Dadson, S. (2021). A regional coupled approach to water cycle prediction during winter 2013/14 in the United Kingdom. *Hydrological Processes*, *35*, e14438. https://doi.org/10.22541/au.161251474.40376313/v1

Mathis, M., Elizalde, A., Mikolajewicz, U., & Pohlmann, T. (2015). Variability patterns of the general circulation and sea water temperature in the North Sea. *Progress in Oceanography*, *135*, 91–112. https://doi.org/10.1016/j.pocean.2015.04.009

McDougall, T. J. (1987). Neutral surfaces. *Journal of Physical Oceanography*, *17*(11), 1950–1964. https://doi.org/10.1175/1520-0485(1987)017<1950:ns>2.0.co;2

Meyer, E. M., Pohlmann, T., & Weisse, R. (2011). Thermodynamic variability and change in the North Sea (1948-2007) derived from a multidecadal hindcast. *Journal of Marine Systems*, *86*(3–4), 35–44. https://doi.org/10.1016/j.jmarsys.2011.02.001

Munchow, A., & Garvine, R. W. (1993). Dynamical properties of a buoyancy-driven coastal current. *Journal of Geophysical Research*, *98*(C11), 20063–20077. https://doi.org/10.1029/93jc02112

O'Dea, E. J., Arnold, A. K., Edwards, K. P., Furner, R., Hyder, P., Martin, M. J., et al. (2012). An operational ocean forecast system incorporating NEMO and SST data assimilation for the tidally driven European North-West shelf. *Journal of Operational Oceanography*, *5*(1), 3–17. https://doi.org/10.1080/1755876X.2012.11020128

O'Dea, E. J., Furner, R., Wakelin, S., Siddorn, J., While, J., Sykes, P., et al. (2017). The CO5 configuration of the 7 km Atlantic Margin Model: Large-scale biases and sensitivity to forcing, physics options and vertical resolution. *Geoscientific Model Development*, *10*(8), 2947–2969. https://doi.org/10.5194/gmd-10-2947-2017

ODYSSEA-Team. (2020). ODYSSEA satellite sea surface temperature, Issue 1.3 [Dataset]. SST ATL SST L4 REP OBSERVATIONS 010 026. https://doi.org/10.48670/moi-00153

Palmer, M. R. (2010). The modification of current ellipses by stratification in the Liverpool Bay ROFI. *Ocean Dynamics*, *60*(2), 219–226. https://doi.org/10.1007/s10236-009-0246-x

Polton, J. A., Palmer, M. R., & Howarth, M. J. (2011). Physical and dynamical oceanography of Liverpool Bay. *Ocean Dynamics*, *61*(9), 1421–1439. https://doi.org/10.1007/s10236-011-0431-6

Porter, M., Dale, A. C., Jones, S., Siemering, B., & Inall, M. E. (2018). Cross-slope flow in the Atlantic Inflow Current driven by the on-shelf deflection of a slope current. *Deep-Sea Research Part I Oceanographic Research Papers*, *140*(August), 173–185. https://doi.org/10.1016/j.dsr.2018.09.002

Rabe, B., Gallego, A., Wolf, J., O'Hara Murray, R., Stuiver, C., Price, D., & Johnson, H. (2020). Applied connectivity modelling at local to regional scale: The potential for sea lice transmission between Scottish finfish aquaculture management areas. Estuarine. *Coastal and Shelf Science*, *238*(March), 106716. https://doi.org/10.1016/j.ecss.2020.106716

Rintoul, S. R. (2018). The global influence of localized dynamics in the Southern Ocean. *Nature*, *558*(7709), 209–218. https://doi.org/10.1038/s41586-018-0182-3

Roquet, F., Madec, G., Brodeau, L., & Nycander, J. (2015). Defining a simplified yet "Realistic" equation of state for seawater. *Journal of Physical Oceanography*, *45*(10), 2564–2579. https://doi.org/10.1175/JPO-D-15-0080.1

Sentchev, A., & Korotenko, K. (2005). Dispersion processes and transport pattern in the ROFI system of the eastern English Channel derived from a particle-tracking model. *Continental Shelf Research*, *25*(18), 2294–2308. https://doi.org/10.1016/j.csr.2005.09.003

Serreze, M. C., Barrett, A. P., Slater, A. G., Woodgate, R. A., Aagaard, K., Lammers, R. B., et al. (2006). The large-scale freshwater cycle of the Arctic. *Journal of Geophysical Research*, *111*(11), 1–19. https://doi.org/10.1029/2005JC003424

Sheehan, P. M., Berx, B., Gallego, A., Hall, R. A., Heywood, K. J., & Hughes, S. L. (2017). Thermohaline forcing and interannual variability of northwestern inflows into the northern North Sea. *Continental Shelf Research*, *138*(November 2016), 120–131. https://doi.org/10.1016/j.csr.2017.01.016

Sheehan, P. M., Berx, B., Gallego, A., Hall, R. A., Heywood, K. J., & Queste, B. Y. (2020). Weekly variability of hydrography and transport of northwestern inflows into the northern North Sea. *Journal of Marine Systems*, *204*(August 2019), 103288. https://doi.org/10.1016/j.jmarsys.2019.103288

Simpson, J. H. (1993). Periodic stratification in the rhine ROFI in the North sea. *Oceanologica Acta*, *16*(1), 23–32.

Simpson, J. H. (1997). Physical processes in the ROFI regime. *Journal of Marine Systems*, *12*(1–4), 3–15. https://doi.org/10.1016/S0967-0653(98)80023-9

Smagorinsky, J. (1963). General circulation Experiments with the primitive equations. *Monthly Weather Review*, *91*(3), 99–164. https://doi.org/10.1175/1520-0493(1963)091⟨0099:gcewtp⟩2.3.co;2

Souza, A. J., & Simpson, J. H. (1997). Controls on stratification in the Rhine ROFI system. *Journal of Marine Systems*, *12*(1–4), 311–323. https://doi.org/10.1016/S0924-7963(96)00105-4

Sündermann, J., & Pohlmann, T. (2011). A brief analysis of North Sea physics. *Oceanologia*, *53*(3), 663–689. https://doi.org/10.5697/oc.53-3.663

Tanguy, S., Jerome, G., Sylvie, P., & Gilles, R. (2020). CORA, Coriolis Ocean Dataset for reanalysis, issue 1.14 [Dataset]. INSITU GLO PHY TS DISCRETE MY 013 001. https://doi.org/10.17882/46219

Tanguy, S., Jerome, G., Sylvie, P., & Gilles, R. (2022). Coriolis Ocean dataset for reanalysis (CORA) july 2022 release, full time series. https://doi.org/10.17882/46219#95183

Thompson, A. F., & Garabato, A. C. (2014). Equilibration of the Antarctic circumpolar current by standing meanders. *Journal of Physical Oceanography*, *44*(7), 1811–1828. https://doi.org/10.1175/JPO-D-13-0163.1

Thomson, R. E., & Emery, W. J. (2014). *Data analysis methods in physical oceanography* (3rd ed.). Newnes.

Tonani, M., Sykes, P., King, R. R., McConnell, N., Péquignet, A. C., O'Dea, E., et al. (2019). The impact of a new high-resolution ocean model on the Met Office North-West European Shelf forecasting system. *Ocean Science*, *15*(4), 1133–1158. https://doi.org/10.5194/os-15-1133-2019

Turrell, W. R., Henderson, E. W., Slesser, G., Payne, R., & Adams, R. D. (1992). Seasonal changes in the circulation of the northern North Sea. *Continental Shelf Research*, *12*(2–3), 257–286. https://doi.org/10.1016/0278-4343(92)90032-F

Wolf, J., Yates, N., Brereton, A., Buckland, H., De Dominicis, M., Gallego, A., & O'Hara Murray, R. (2016). The Scottish shelf model. Part 1: Shelf-wide domain. *Scottish Marine and Freshwater Science*, *7*(3), 151. https://doi.org/10.7489/1692-1

Zijl, F., Verlaan, M., & Gerritsen, H. (2013). Improved water-level forecasting for the Northwest European shelf and north Sea through direct modelling of tide, surge and non-linear interaction topical collection on the 16th biennial workshop of the Joint numerical sea modelling group (JONSMOD) in Bre. *Ocean Dynamics*, *63*(7), 823–847. https://doi.org/10.1007/s10236-013-0624-2